MECHANICAL PROPERTIES OF THERMAL SPRAY COPPER ALLOYS COATINGS

BY

MOHAMED ELHADI MOHAMED IBRAHIM

A Thesis Presented to the
DEANSHIP OF GRADUATE STUDIES

KING FAHD UNIVERSITY OF PETROLEUM & MINERALS

DHAHRAN, SAUDI ARABIA

In Partial Fulfillment of the
Requirements for the Degree of

MASTER OF SCIENCE

In

MECHANICAL ENGINEERING

MAY 2016

KING FAHD UNIVERSITY OF PETROLEUM & MINERALS

DHAHRAN- 31261, SAUDI ARABIA

DEANSHIP OF GRADUATE STUDIES

This thesis, written by MOHAMED ELHADI under the direction his thesis advisor and approved by his thesis committee, has been presented and accepted by the Dean of Graduate Studies, in partial fulfillment of the requirements for the degree of **MASTER OF SCIENCE IN MECHANICAL ENGINEERING**

Dr. Khaled Saleh Al-Athel
(Advisor)

Dr. Zuhair Gasem
Department Chairman

Dr. Abul Fazal M. Arif
Member)

Dr. Salam A. Zummo
Dean of Graduate Studies

Dr. Syed Sohail Akhtar
(Member)

17/05/2016
Date

To me in the Future

ACKNOWLEDGMENTS

I would like to deliver my sincere thankfulness and gratitude to my family for supporting me during my study.

Special thanks to my academic advisor Dr. Khaled Saleh Al-Athel for his endless motivations, supports and advises.

Special thanks to my committee members Dr. Abul Fazal Aril and Dr. Syed Sohail Akhtar for insightful and inspiring comments and advises.

I also would like to convey my deep gratitude to King Fahd University represented in their administration for giving me the opportunity to pursue my graduate study, providing all necessary tools for me to become a good researcher, and leading our Region in the scientific arena.

I would not forget to thank Sudanese Community at King Fahd University for their support during my study.

TABLE OF CONTENTS

LIST OF TABLES

LIST OF FIGURES

LIST OF ABBREVIATIONS

TS	:	Thermal Spraying.
HVOF	:	High Velocity Oxygen Fuel.
PS	:	Plasma Spraying.
TBC	:	Thermal Barrier Coatings.
TGO	:	Thermally Grown Oxide.
YSZ	:	Yttria Stabilized Zirconia.
CACT	:	Center of Advanced Coating Technologies.
FEA	:	Finite Element Analysis.
SEM	:	Scanning Electron Microscopy.
XRD	:	X-ray Diffraction.
OM	:	Optical Microscope.
EDS	:	Energy Dispersive X-ray Spectroscopy.
GDOES	:	Glow Discharge Optical Emission Spectrometry.
XPS	:	X-ray Photoelectron Spectroscopy XPS.
EPMA	:	Electronic probe microanalysis.

ABSTRACT

Full Name : [MOHAMED ELHADI MOHAMED IBRAHIM]

Thesis Title : [MECHANICAL PROPERTIES OF THERMAL SPRAY COPPER ALLOYS COATINGS]

Major Field : [MECHANICAL ENGINEERING]

Date of Degree : [MAY 2016]

Thermally sprayed Copper and Copper Alloys coatings are among the widely applied coating materials for several industrial and medical applications to serve various functions such as corrosion resistance, wear resistance. Along with silver, copper and copper alloys coatings are recently being utilized for antibacterial coating applications. In the present study, microstructure and mechanical properties, namely, adhesion strength, hardness, and scratch resistance of Cu, Cu 4%Sn, Cu 17%Ni 10%Zn (German Silver) and Cu 17%Al 1%Fe (Aluminum Bronze) are investigated experimentally. All coatings are deposited on stainless steel substrate disks of 25mm diameter using Wire Arc spraying technique at the center of advanced coating technologies (CACT), University of Toronto. SEM is used to study the microstructure of the coatings. Surface roughness is also measured using 3D profilometer. Adhesion strength is evaluated using pull-off adhesion test, whereas hardness and scratch resistance are investigated using instrumented micro-indentation and micro-scratch tester respectively. It was found that Cu 17%Al 1%Fe has highest adhesion strength, hardness, and scratch resistance among all tested compositions. It also found that the adhesion strength decreases as the coating thickness increases, whereas scratch and indentation hardness increases with the thickness of the

coating. Comparison and discussion of these coatings and the effect of their thickness are presented accordingly.

ملخص الرسالة

الاسم الكامل: **محمد الهادي محمد إبراهيم**

عنوان الرسالة:

التخصص: هندسة ميكانيكية

تاريخ الدرجة العلمية: **إبريل 2016**

الطلاء المعدني بالنحاس وسبائكه يستخدم على نطاق واسع لعدة تطبيقات في المجالات الصناعية والطبية لخدمة وظائف مختلفة مثل مقاومة التآكل، و غيرها. في الاونة الاخيرة، أثبتت بعض التجارب ان طلاءات النحاس و سبائكه لها القدرة علي قتل الجراثيم، و لذك يمكن استخدامها كطلاءات مضاده للجراثيم في المستشفيات و المرافق العامة. في هذه الرسالة، يتم دراسه خواص المادة المجهرية والخواص الميكانيكية وهي قوة التصاق، والصلابة، ومقاومة المادة للخدش عن طريق التجارب المعملية لاربع طلاءات معدنية نحاسية مختلفة و هي النحاس الخالص والنحاس مع 4٪ من القصدير والنحاس مع 17٪ من النيكل و 10٪ من الزنك والنحاس مع 17٪ من الالمنيوم و 1٪ من الحديد. كل هذه المواد مطلية علي اقراص من الفولاذ المقاوم للصدأ قطرها 25 مم. تم تصنيع هذه العينات بواسطه الطلاء بالرش الحراري في المركز المتقدم لتكنولجيا الطلاء بجامعة تورنتو في كندا. لدراسة الخواص المجهرية لهذه المواد، تم إستخدام المجهر الإلكتروني (SEM). أيضا تم قياس خشونة السطح أيضا باستخدام جهاز قياس السطح ثلاثي الأبعاد (profilometer 3D). أما فما يتعلق بالخواص الميكانيكية فقد تمت دراسة قوة التصاق باستخدام إختبار السحب العمودي للإتصاق، في حين تمت دراسه صلابة المواد و مقاومتها للخدش باستخدام اختبار التسنن (indentation) و اختبار الخدش على التوالي. تبين أن طلاء سبيكة النحاس مع 17٪ من الالمنيوم و 1٪ من الحديد لديها أعلى قوة التصاق و صلابة، ومقاومة للخدش بين جميع السبائك الاخري. كما وجد أن قوة التصاق تقل كلما يزيد سمك الطلاء،

في حين أن صلابة الخدش تزيد مع زيادة سمك الطلاء. وفقا لذلك، تمت مقارنة ومناقشة هذه الطلاءات وتأثير سمكها علي الخواص الميكانيكية.

CHAPTER 1

INTRODUCTION

Coatings are extensively being applied in many areas including industrial and medical fields. The applied coatings can function as corrosion resistance, wear resistance, or in other areas like in semiconductor device fabrication. The coatings add a completely new property to the substrate, so the coating may form an essential part of the final product. Copper and copper alloys coatings are among the widely applied coating materials for several industrial and medical applications to serve various functions. Thermally sprayed copper and copper alloys coatings are also being utilized for antibacterial coating applications [1]. The performance of these coatings is usually related to their microstructure, tribological and surface characteristic [1-5]. Therefore, the study of microstructure and mechanical properties of these coatings is of great importance.

In this chapter, an introduction to coatings, their deposition techniques, and their common application is presented. This is followed by a discussion on mechanical properties that are important to coating systems. Finally, copper and copper alloys to be studied in this thesis will be briefly discussed along with the goals of this research.

1.1 Background: Coating Systems

A Coating can be defined as a layer of material that covers a certain object. The covered object is referred to as the substrate. The thickness of the coating layer can extend from few nanometers to millimeter scale depending on the application. It is also common that

more than one layer of coatings is applied for certain applications. Figure 1-1 shows an example of the coating substrate systems.

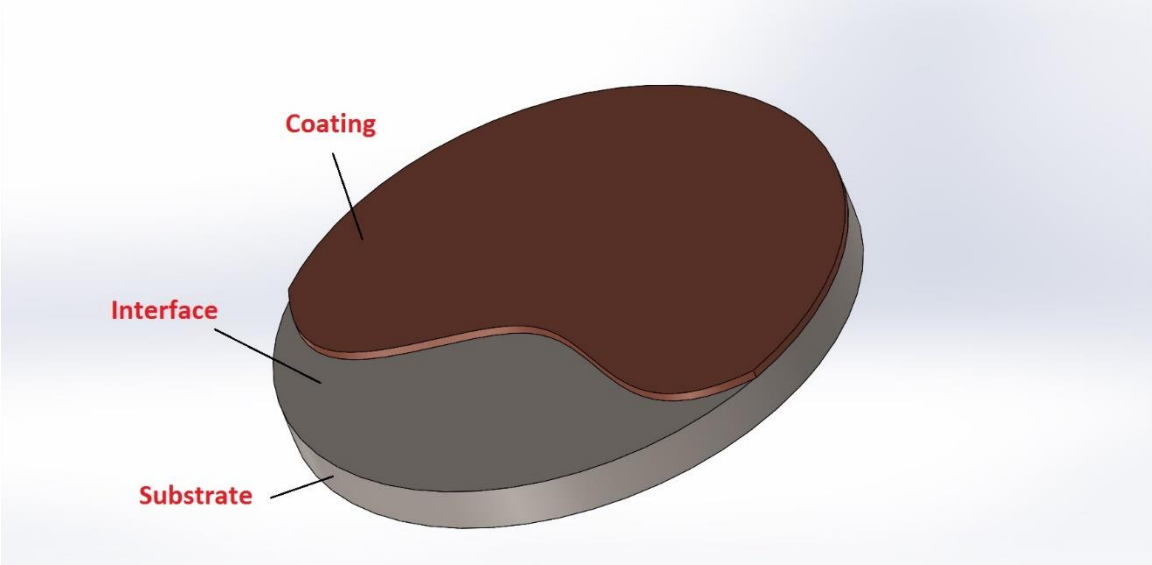

Figure 1-1 Coating-substrate system.

The essence of using coatings is that a coating may add a completely new property to the substrate, and therefore it may form an essential part of the final product.

1.2 Coating Manufacturing Processes

The process of producing a coating and bonding it to the surface of a substrate is called deposition process. These processes are a bit complicated because they are required to produce a certain thickness of the coating layer, to ensure the bonding of the coating to the surface of the substrate, and to result in minimum damages to the surface microstructure of the substrate. There are many processes or techniques by which coating may be applied and bonded to the surface of the substrate including, Chemical Vapor Deposition (CVD), Physical Vapor Deposition (PVD), Roll-to-Roll coating process, cold spraying, and thermal spraying. Physical vapor deposition PVD consists purely of

physical processes, in which the material to be coated is removed by sputtering or evaporation, then transported to the surface of the substrate, then condensed under vacuum on the substrate surface and forms the coating layer. Many processes lie under the umbrella of the PVD process, they are named according to the physical vapor source, for example, diode or triode sputtering, ARC evaporation, activated reactive evaporation, electron beam evaporation, planar or cylindrical magnetron sputtering, and direct current (DC) or radio frequency (RF) sputtering. Typical PVD deposition temperatures range from 450 to 550 ^{o}C. PVD techniques have the ability to control the thickness of the coating and also, the produced coatings have high compressive residual stresses that hinder the formation and growth of cracks. Ability to utilize various types of coating materials for various types of substrates with an environmentally processing is among the beneficial characteristics of the PVD Techniques. Unlike PVD, chemical vapor deposition CVD is based on reactions or decomposing of gaseous chemical compounds on the surface of the substrate to produce the desired coating film. These chemical reactions involve a transfer of heat energy, and usually, the substrate is preheated and kept at higher temperatures compared to the other components of the system. In CVD, the deposition temperature plays an important role in the grain size and the thickness of the resulted coating. Typically, the deposition temperatures vary from 800 to 1200 ^{o}C. Usually, lower temperatures are desirable. Plasma assisted CVD (PA-CVD) is employed to reduce the temperature required for the reaction, where the substrate is exposed to an electrical plasma in the gas phase during the deposition process. CVD has the ability to produce thick coating layers at the high deposition rates [3].

1.3 Thermal Spray Coatings (TS)

Thermal spraying processes are among the widely applied coating deposition techniques. In thermal spraying, a heat source is utilized to melt the coating material that is usually fed in form of powder or wire, then the molten or semi-molten material is propelled and sprayed onto the surface of the substrate. The particles temperature decrease rapidly (quench) after it hits the substrate surface, subsequent particles build up over each other creating the final thickness of the coating. The source of energy in thermal spraying processes can be chemical (by means of combustion), or electrical such plasma or arc. A wide range of materials can be deposited with thermal spraying include alloys, metals, ceramics, composites, and plastics. There are five commercially available spraying methods discussed next.

1.3.1 High Velocity Oxygen Fuel (HVOF)

Developed during the 1980s. The HVOF gun consists of a combustion chamber that is fed with a fuel (liquid or mixture of gases) and oxygen, then the fuel is ignited inside the combustion chamber continuously. Typically, the fuel may be propane, propylene, natural gas, hydrogen. Kerosene and acetylene may also be used as a combustion fuels. Hot gases result out of this combustion process may have a pressure up to 1 GPa. These hot gases flow through a converging-diverging nozzle with a very high gas velocity that it can reach up to 2100 m/s. The coating material is fed into these hot gas streams in form of powders, and since the gases have high velocity, this results in high particles velocity, typically between 400 and 800 m/s. The injected powder is partially melted in the stream and then the whole stream is directed to the substrate surface. These high velocities result mainly in achieving a greater coating density. It also produces coatings with a less

porosity, high bonding strength, improved thickness capability, lesser environmental effects and improved surface finish. This process is mainly used to deposit corrosion resistant and wear resistant coatings. Typical coatings powders are chromium carbide (WC-Co), and alumina (MCrAlY). The temperature range in HVOF is 2500 -3000 ^{o}C depends on the combustion gases [4].

1.3.2 Flame Spraying

In this process, the coating material is combusted until it melts then sprayed into the substrate surface. The most commonly used type of fuel is oxygen-acetylene, oxy-hydrogen or oxy-propane. The temperature of the combustion flame reaches 3000 ^{o}C depending on the fuel ratio. Coating Materials can be fed in three forms: powder, wire, or rod-flame spray. The velocity of the particles is relatively low, and it varies from 40-100 m/s depending on particles density and shape. These low velocities result in coatings that have inclusions inside its structure and high level of porosity.

Several coating materials can be deposited with flame spraying, including Zinc and Aluminum deposited on steel for anti-corrosion coatings, Nickel/Aluminum composite wire for the purpose of bond coats and the so-called self-bonding coatings, also Molybdenum for bond coats, High Chromium steel for several applications, and nickel/aluminum for heat and oxidation resistance [4].

1.3.3 Detonation

Developed during the 1960s. The detonation process is formed in a detonation gun, which consists of a long water-cooled tube or barrel that has inlet valves for the gases and the coating material that fed in form of powders. The most common used type of fuel in

this process is acetylene, which is fed along with the oxygen into the barrel through separate valves, and the charge of the powder is fed through the another valve. The mixture is then ignited by a spark, which makes a detonation inside the barrel that results in accelerating the powder. Nitrogen is fed in form of pulses to clean the barrel of combustion residuals after each detonation process. The process of detonation is based on repetitive explosions instead of continuous combustion, and it is reported that these explosions or detonations together with the subsequent cleaning are repeated many times in one second. The velocity of the mixture can reach up to 1200m/s with very high temperatures inside the tube that may attain 4000^{o}C. This high kinetic energy gives a very dense and strong coating. Every shot will create a certain thickness of the coating, this thickness depends on the size of the particles, frequency, gas flow rate, the ratio of the combustion gases and the distance between the substrate and gun [5].

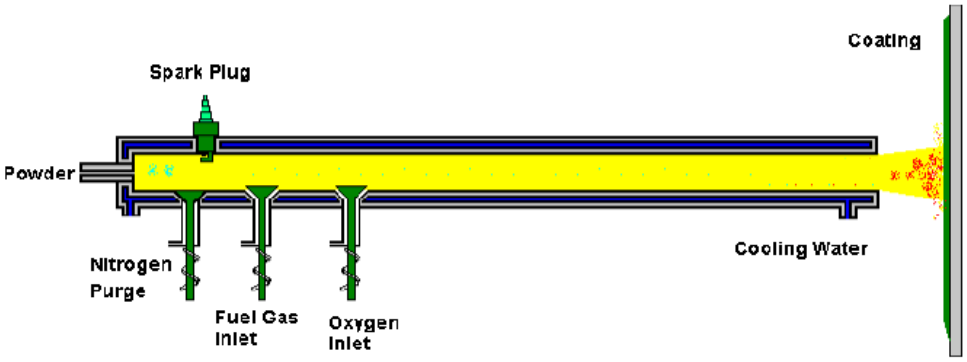

Figure 1-2 Schematic of detonation gun

1.3.4 Wire Arc Spraying

In this process, two individual metal wires are fed to the spray gun independently, then they are charged electrically and an “arc” is created between them. A large amount of

heat is generated by this arc (the arc acts as a heat source) where the temperature may attain 4000^{o}C with a current density of 100 A/mm^{2}. This results in melting the incoming wire material. After the wires are melted, it is entrained from the gun to the air jet with particle velocity that reaches 150m/s. This entrained molten material is then deposited onto the substrate, as shown in Figure 1-3.

Wire arc spray coatings are more commonly used in heavy and metallic coatings, and it can be found in many applications like anti-corrosion coatings of zinc and aluminum, wear resistance, dimensional restoration and others. Wire arc spraying generally produces denser and stronger coatings, and usually, the process of arc spraying has low running cost with a high efficiency. However, not all material can be used in arc spray coating but only electrically conductive wire [4].

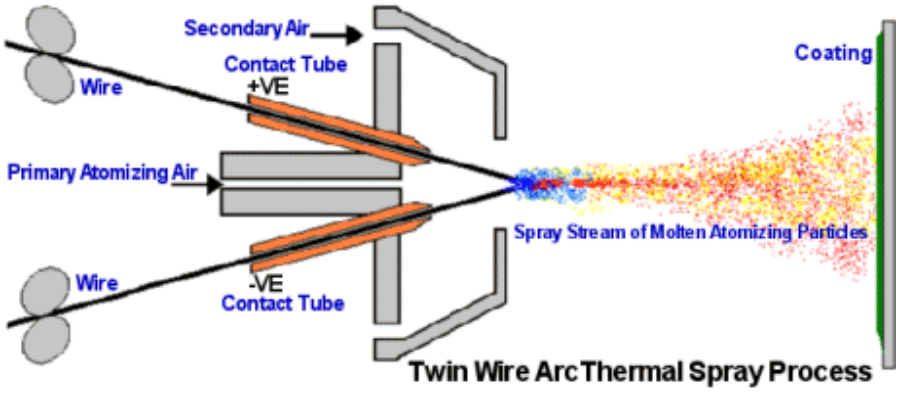

Figure 1-3 Schematic of wire arc spraying process

1.3.5 Plasma Spraying (PS)

In this spraying process, a gas, usually argon, is allowed to move between a cathode and anode. The cathode is usually tungsten and the anode is copper. By using a high-frequency discharge, an electric arc is created between the cathode and the anode. The created arc ionizes the argon gas creating a gas plasma with a high pressure and ultra-

high temperature that may reach 30,000 °C, which in turn increases the velocity of the gases at the exit of the nozzle creating a plasma torch with a power of 30 to 80 kW. The coating material is then fed in form of powder into the gas stream, where it is heated and accelerated by the plasma gas. The powder velocity and temperature are determined by the design of the torch and operating parameters not only such as powder feed rate, carrier gas flow, powder size, and gas flow but also the deposition angle and distance from the substrate to the torch (standoff distance).

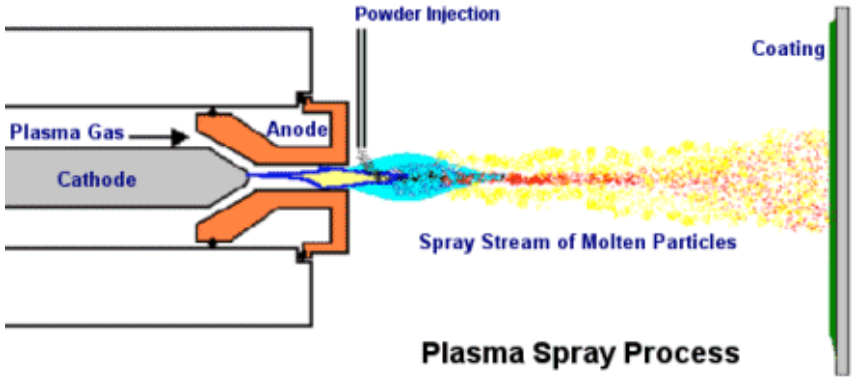

Figure 1-4 Schematic of plasma spraying process.

Typically, the velocity of the powder is between 300 and 550 m/s with a melting or slightly above temperatures. In addition to the velocity and temperature, how the powder particles react with the surrounding gases is of importance. If spraying is taking place in air, extensive oxidation of the powder particles may occur which will result in drastic reduction in the bond strength, coating density, and cohesive strength. This can be avoided by setting suitable operating parameters at the torch, selecting and adequate standoff, and using effective gas shrouding or inert gas chamber. Inert-atmosphere plasma spraying in low-pressure chamber is the most commonly used technique because it has many unique features including standoff independent deposition and oxidation-free

substrate preheating which results in better bond strength and greater control of the residual stress. The resulting coating of plasma spraying deposition will typically have 34 up to 70 MPa bond strength, and 0.05 to 0.5 mm thickness [6].

1.4 Applications of Thermal Spray Coatings

Coatings are applied extensively in industry because they provide solutions for many problems. Typical applications of thermal sprayed coatings are briefed next.

1.4.1 Wear Resistance

There are several wear mechanisms including abrasion, cavitation, adhesion wear, and fretting all of which can be avoided by means of coating. This is the most common use of thermally spray coatings where, by application of the suitable coating, wear can be controlled or retarded. Applied coatings are usually ceramics or any other materials that are harder than the material of the object.

1.4.2 Corrosion Resistance

Corrosion can be seen as the gradual destruction of a material by means of chemical reaction with the surrounding environment. It usually happens in metals and takes place when high velocity fluids (gases or liquids) and particulate solids are exposed to the surface of a metal. These fluids prevent the formation of protective oxides and allow the corrosion to take place. Coating is the most common anti-corrosion remedy. It provides a protective layer or barrier between the material and the corrosive environment.

1.4.3 Thermal Barrier Coatings (TBC)

Some applications of metallic surfaces usually require them to operate at very high temperatures, more than 800 ^{o}C as in gas turbine or aero-engine. Such high temperatures

can easily cause hot corrosion, oxidation, thermo-mechanical fatigue, and creep. Thermal Barrier Coating TBC is an arrangement of advanced materials that consist of three layers. the topmost one is a ceramic layer, usually Yttria-stabilized Zirconia (YSZ). This ceramic layer creates the largest thermal gradient of the TBC and keeps the lower layers at a lower temperature than the surface stabilized zirconia. The second layer is bond coat layer, which is usually a metallic layer of platinum aluminide. The third layer is the Thermally Grown Oxide (TGO), which is a thick layer of oxide, predominantly AL_2O_3. This layer is created during the process of deposition of the ceramic coating on the bond coat surface. These layers together can dramatically reduce the high operating temperatures and prevent the structure from thermal fatigue and creep and thus, enhance the life of the components.

1.4.4 Dielectric Coatings

In some lenses or mirrors, a thin layer of coating is usually applied to change the reflection capability of the optical surface. Using such type of coating allows the reflectivity of the optical surface to vary from zero (anti-reflection coating) to 99.99% (high-reflective coating). Materials such as oxide ceramics are usually used as dielectric coatings in electronic devices.

1.4.5 Antibacterial Coatings

Biofilm formation and bacterial colonization are serious issues in food processing, medicine, surgical tools, and others. Adhesion of the bacteria to surfaces plays an important role in tissue infection, ship fouling, dental decay, fermentation, and sewage treatment [7]. One of the effective methods or strategies to reduce microbial numbers on healthcare surfaces is to apply a coating with both antibacterial behavior and low surface

energy. When the surface energy is low, attachment of microbial bodies will be minimized while antibacterial properties inhibit the growth of the bacteria. The attachment and growth of bacteria are influenced by several parameters including, the chemical composition of the coating, coating thickness, surface topography and morphology, type of bacteria and their characteristic and the surrounding environment such as temperature and the medium [7]. Several metals are proven to show some antibacterial capabilities like gold, silver, zinc and copper [2]. Some of these materials are available in the market [8]. Usually, thermal spraying techniques are used to deposit the antibacterial coatings.

1.5 Mechanical Properties of Coatings

There are some properties that markedly determine the quality and performance of the coating system during service life. Some of these properties are discussed next.

1.5.1 Coating Adhesion

Coated parts sometimes are viewed as systems that consist of three main components, the coating material, the base material for which the coating is applied (the substrate), and the interface (adhesion layer) between the coating and the substrate, as shown in Figure 1-1. The property of adhesion assesses the degree to which the coating is attached or glued to the surface of the substrate. It is usually evaluated by measuring the force or strength required to detach the coating completely from the substrate. These forces are assumed to act neither upon the coating nor the substrate, but at the interface between them. This is because, in many cases, the coating substrate interface is the weakest part of the coating system.

There are many factors affecting the interface adhesion between the coating and the substrate including chemistry and physics of the surface, type of substrate and coating materials, the stresses in the substrate, and the method through which the coating is applied. Several experimental methods are used to study the coating-substrate adhesion including Scratch test, Tension test, Micro-indentation test, three-points bending test and Pull-off test.

1.5.2 Coating Hardness

In general, Hardness is defined as the material's ability to resist plastic deformation due to surface penetration. This definition is usually extended with according to the way through which force is applied and how the hardness is measured. As far as the coating systems are concerned, hardness is defined as the resistance to plastic deformation during scratching and indentation. Measurements of hardness may said to be macro-, micro-, or nano- according to the applied forces and obtained displacements. The most common type of hardness measurement in coating applications is the indentation test. Usually, indentation is performed on the cross section of the coating systems to assess the interface hardness as well as to study the change of hardness with the distance from the interface (hardness profile). Evaluation of the hardness profile is of great importance for some coating applications such wear resistance coating.

1.5.3 Scratch Resistance

Coating resistance to scratch is of paramount importance to coating quality and performance during real life applications. There has been a constant demand for enhanced surface integrity and minimized damage of coatings, which strongly affect the mechanical and physical properties and hence, degrade quality and performance of the

coated part. This has acted as a driving force for the continuous study of plastic deformation caused by scratching of coatings [9].

1.6 Residual Stresses in Thermally Sprayed Coatings

These are the stresses that exist in the coating in free load condition. Residual stresses are formed during the deposition process of the coatings. Many parameters contribute to the formation of the residual stresses like deposition temperature, the kinetic energy of the coating particles, the cooling rate, thermal expansion mismatch between the coating and the substrate and the strain rate behavior of both the coating and substrate materials. Residual stress profile can also change during the service of the coated component due to loading or any post-treatment. There are many experimental techniques used to evaluate the residual stresses in coating systems. These techniques may be classified into three groups. Non-destructive techniques like neutron diffraction, synchrotron X-ray, and XRD. Semi-destructive like layer removal and hole drilling, other miscellaneous techniques like four points bending and Almen strip.

1.7 Copper and Copper Alloys

Thermally sprayed Copper and Copper Alloys coatings are used in many applications including corrosion resistance, antifriction surfaces (bearing surface), and recently for antibacterial applications. Some of the copper alloys that will be used in this study are briefly discussed in this section.

Copper

Copper lies within group 11 in the periodic table, therefore, it has one s-orbital electron on the top of a filled d-electron shell. Copper is characterized by high electrical

conductivity, high ductility, and good corrosion resistance. Copper also possesses a high thermal conductivity, and it comes as the second highest after silver among pure elements at room temperature. The high thermal and electrical conductivity of copper can be partially explained by the softness of this elements.

Copper is obtained from copper ores that are usually found in mines as sulfides. The ores are crushed and the metal components of the powder are separated, from which copper is extracted. Copper is then melted and purified up to 99%. The structure of the cast copper is of dendritic nature. However, when copper is hot rolled, the interdendritic structure is completely destroyed.

Copper-Tin alloys

Tin bronzes or copper-tin alloys are best known for their performance as corrosion resistant materials, they also have high wear resistance and low coefficient of friction especially against steels. They are used in several applications such as in bearings, piston rings, gears, valves, and fittings.

Tin bronzes usually contain 1.5 - 9% Sn and 0.01-0.4% P. They are usually wrought materials, and their microstructure usually consists of cored dendrites. These dendrites have a composition gradient of increasing tin concentration as they grow. Tin is considered as a solid solution strengthener in copper, despite the fact that it has low solubility in copper, especially at room temperature. Lead is sometimes added to the tin bronze to the pressure tightness and machinability, however, it decreases the tensile strength and ductility of the alloy.

German Silver

German silvers, nickel silvers or nickel brasses are alloys that contain copper, nickel and zinc. They are featured by an attractive silver luster. These alloys have moderated strength and good corrosion resistance. They are found in many application as food and beverage handling equipment, electroplated tables, musical instruments, zippers, costume jewelry, and optical equipment.

The microstructure of nickel silver is predominantly single phase solid solution. The percentage of alloy component is usually 7 to 20% nickel and 14 to 46% zinc. Nickel is soluble in copper, so it usually remains in solid solution with the copper, however, zinc has limited solubility in copper. When the alloy contains a high percentage of zinc, it usually becomes two phases.

Aluminum Bronze

Besides their excellent corrosion resistance, Aluminum bronzes are known for their high strength and good corrosion resistance. The presence of aluminum in the alloy is what gives the bronze its spectacular corrosion resistance, where the aluminum reacts with oxygen in the atmosphere to form a thin layer if alumina, which acts as a barrier to corrosion.

Aluminum bronzes typically contain between 9-12% Aluminum and a percentage of iron that can reach up to 6%. These alloys are usually hardened by a combination of cold work, solid solution strengthening, and precipitation of an iron rich phase. They are used in many applications such as machine tool ways and heavy duty sleeve bearings.

Usually, standards Cu-Al-Fe alloys are cast material and the percentage of the Al in the alloy is limited to 12% as maximum. Spray-forming enables incorporation of high

aluminum content in the alloy (up to 18%), which in turns, increases the mechanical strength of the alloy [10]. Moreover, when aluminum bronze is thermally sprayed on a surface of steel substrate, metallurgical interactions could occur between the bronze and the steel, which is the often the reason behind the high bond strength of the aluminum bronzes [11].

1.8 Research Goals

Coatings in general, as we introduced in the previous sections, are applied to a certain surface to serve a specific function such as corrosion resistance, wear resistance, etc. Therefore, material selection, design, and manufacturing of coatings are carried out with regard to the desired application. Performance evaluation tests are then conducted to assess the quality of the produced coatings. Coating performance examination can be divided into two stages; first, functional evaluation i.e. testing the coating's ability to meet the required application (corrosion test, wear test, antibacterial test, etc.). Then, it is of importance for a coating to possess good mechanical properties such as adhesion to the substrate, hardness, scratch resistance, etc. Figure 1-5 shows a flow chart of coating design and performance evaluation.

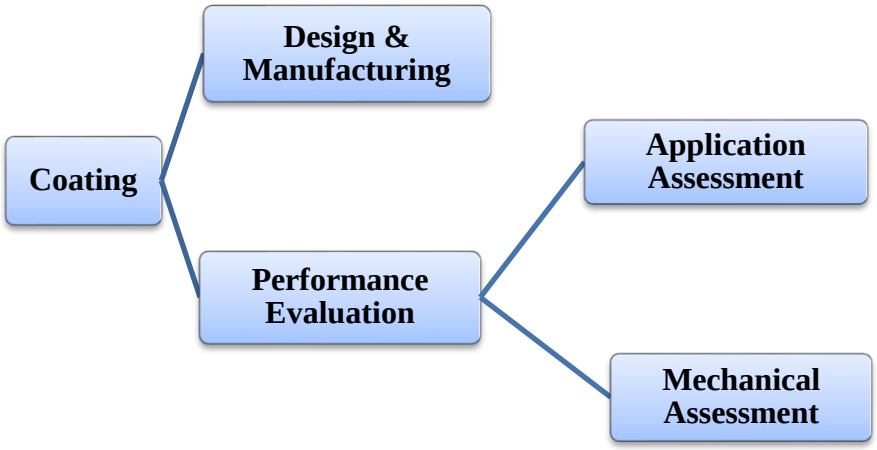

Figure 1-5 Coating design and assessment

Thermally sprayed Copper and Copper Alloys coatings, along with Silver and Zinc, have shown to have good antibacterial capabilities. Having these coating applied to a certain surface for the antibacterial purpose, they are required to perform efficiently from a mechanical point of view, i.e. they should have good adhesion to substrate surface, good hardness and scratch resistance, etc. Therefore, mechanical properties of these coatings need to be studied and a compromise should be made between antibacterial behaviors and the mechanical properties.

In the present study, microstructure and mechanical properties of copper alloys coatings are to be investigated experimentally. The coating materials to be studied are pure copper and several copper alloys as shown in Table 1-1.

Table 1-1 Available coated samples.

Coating composition	Coating thickness
Copper	150

Copper-Tin-Phosphorus	150
Copper-Aluminum-Iron (Aluminum Bronze)	150
	200
	300
Copper-Nickel-Zinc (German silver)	150
	200
	400

All coatings are deposited on stainless steel substrate disks of 25mm diameter. Three different thickness are available for Copper-Nickel-Zinc (German silver) and Copper-Aluminum-Iron (Aluminum Bronze) coatings, as indicated in Table 1-1. The samples were manufactured at the center of advanced coating technologies (CACT), University of Toronto using Wire Arc spraying technique. The mechanical properties to be assessed are adhesion, hardness, and resistance to scratch. Adhesion strength will be evaluated using pull-off adhesion test. This test method maximizes the tensile stress from zero to minimum stress required to detach the coating perpendicular to the substrate surface. Hardness will be assessed by using instrumented micro-indentation with Vickers indenter. Scratch hardness will also be measured and compared to the indentation hardness. The roughness of these coatings will also be assessed using 3D profilometer.

CHAPTER 2

LITERATURE REVIEW

In this chapter, a review of the previous works done in assessing microstructure and mechanical properties of coatings. That will be followed by the specific objectives of this research.

2.1 Coatings Characterization

Many techniques can be used to study the microstructure of coatings. Most commonly, Scanning Electron Microscopy (SEM), X-ray Diffraction (XRD), Optical Microscope (OM) are used. Typically, characterization of coatings is done in two stages: First, the powder of the coating material is characterized before the deposition process often with the aim to study the effect of shape and size of powder on the resulting coating. Then, after the deposition process, the coating is looked into to see the formed microstructure, morphology, the phases formed during deposition, etc.

Koivuluoto and Vuoristo [12] used Scanning Electron Microscopy (SEM) to measure the size and morphologies of Cu + Al_2O_3 powder before deposition process to study the effect of Al_2O_3 on the properties of the copper coatings. The amount of the Al_2O_3 in the coating was also measured by SEM. Triantou et al [13] used SEM, in a study of the effects of adding Al_2O_3 to copper coatings on hardness and bond strength, to identify oxides that may be formed during deposition. SEM images showed no oxidation observed in the surface of the coating due to the deposition process. This is the main

advantage of cold spraying over thermal spraying. The images also showed that the copper particles have a flattened shape because of the heavy deformation due to high strain rate caused by high-velocity impact during cold spraying. Almost zero percentage of porosity was reported because of the intense plastic deformation associated with cold spraying process. SEM results were confirmed by X-Ray Diffraction (XRD). Sharifahmadian et al [7], in a study of the relationship between surface properties of copper coatings and antibacterial behavior, used SEM for microstructural analysis and XRD to analyze the coating surface composition. Energy Dispersive X-ray Spectroscopy EDS scan was also performed to verify the results. Their images revealed the existence of some pores and splats, and they concluded that these pores improve the antibacterial properties. Jin et al [14] studied the Microstructure, corrosion and tribological properties of Ti–Cu coated stainless steel, using SEM, XRD and glow discharge optical emission spectrometry (GDOES). Through the images, they discovered that if the concentration of the coating, i.e Ti and Cu, decreases gradually from the surface to the interior, the bond strength and the antibacterial behavior at the surface will be improved. In the work of Culha et al [15] an image analyzer was used along with XRD, OM, and SEM to study the microstructure of thermally sprayed NiAl coatings on stainless steel substrate. They found a pancake shape in of the particles formed by the post-impact, and porosity as small as 2.5%. Excellent homogeneity and uniformity, low oxide content, and high quality contact at the coating-substrate interface were also found. Guo et al [16] used a relatively new characterization technique called X-ray Photoelectron Spectroscopy (XPS) along with energy dispersive X-ray spectrometer EDS and SEM to analyze the composition and the chemical state of Ag–polytetrafluoroethylene antibacterial coatings

on silicon rubber substrate. Jin et al [17] however, used SEM to study the thermal shock in thermal barrier coatings reinforced by different ceramics. SEM images revealed that almost all failures occur at the inner ceramic coating near to the interface of ceramic layer/bond coat. In the work of Wensheng [18], SEM and XRD were used to study the microstructure and of plasma sprayed Ce + Cu-14Al-4.5Fe coatings. Electronic probe microanalysis (EPMA) was also used to examine the micro-constituents of the coating surfaces. Uniform distribution of all constituent elements was reported. Vakili et al [19] used SEM and XPS to characterize epoxy coatings on steel substrates treated by Cerium and Zinc phosphate. Inhomogeneity and visible roughness have been reported for the samples treated with Cerium. They also reported that the composition of the steel substrate was changed due to the post-treatment of the Ce treated sample by Zn.

2.2 Coating Adhesion

The adhesion strength at the coating-substrate interface and the cohesion among the splats, to a large extent, determine the quality of the coating systems. This is because the most common types of coating failures are debonding of the coating from the substrate, and the cracking of the coating itself. While the cohesion bond strength indicates the coating wear behavior, adhesion bond strength primarily assesses the quality of the coatings [20]. Both of them are influenced by the distribution of the residual stresses during the deposition process. This is mainly because residual stresses can change the interface significantly, creating delamination which in worst cases can cause coating spallation [21].

Azizpour et al [21] discussed and compared the techniques used to measure the bond strength for thermally sprayed coatings. Vakili et al [19] used Pull-off test to measure the adhesion strength of epoxy coated st-37 steel that had been treated with cerium and zinc phosphate before the coating was applied. Pull-off tests were done for treated and untreated samples. The treated substrate samples showed higher adhesion strength than the untreated ones, and that the Ce treated had adhesion strength higher than Zn treated samples. Wensheng et al [18] used pull-off test to study the effect of adding Cerium to Cu-14Al-4.5Fe (Aluminum bronze) coating on the bond strength. The Cerium was added to the pre-alloy and then the mixture was atmospherically plasma sprayed on 45 carbon steel substrate. It was found that by adding only 0.6% of cerium, the bond strength increased by 17.4% higher than that of Cu-14Al-4.5Fe without Cerium. Koivuluoto and Vuoristo [12] used the tensile pull test to study the effect of the powder type of copper mixed with Al_2O_3 on the bond strength after the coating establishment. Different coating types were examined and that the coatings prepared from spherical particles had higher bond strength because it had experienced high plastic deformation. Zhong Li et al [11] also used the tensile test to study the adhesion strength of arc sprayed aluminum bronze coatings on a mild steel substrate. They also studied the effect of heat treatment on the bond strength. In the work of Miguel et al [22], the effect of adding alumina to aluminum bronze on the adhesion strength was studied. It was found that adding alumina significantly increases the adhesion strength of the coating because more interface deformation takes place during the deposition. Also in the work of Jin et al [17], the tensile test, which is conceptually similar to the pull-off test, was used to study the effect of adding ceramics on the adhesion strength of thermal barrier coatings. different

ceramics with different percentages were added to the Yttria Stabilized Zirconia (YSZ) to form 5 wt% La_2O_3+3 wt% TiO_2+ 92 wt% YSZ(5La3TiYSZ), 8 wt% La_2O_3+92 wt% YSZ (8LaYSZ) and 8 wt% CeO_2+ 92 wt% YSZ(8CeYSZ). The adhesion test showed that the TBC with 8 wt%La_2O_3 has the lowest adhesion strength and 5La3TiYSZ has the highest one, but all of them found to have an adhesion strength higher than pure TBC. Table 2-1 shows some of the adhesion strength values found in the literature for pull-off and tensile adhesion tests.

Table 2-1 Adhesion Strength values from the literature.

Author	Coating - Substrate	Test Method	Bond Strength (MPa)
Zhong Li et al [11]	Cu 7%Al on Steel substrate	Tensile test	23 - 27
Koivuluoto and Vuoristo [12]	Cu+Al_2O_3 composite coating on Steel substrate	Pull -off test	6 - 20
Vakili et al [19]	Epoxy on steel substrate	Pull -off test	2.3 – 3.5
Wensheng et al [18]	Cu-14Al-4.5Fe on steel substrate	Cylindrical tensile test	290 - 350
Miguel et al [22]	Cu10%Al1%Fe+Alumina composite coatings on mild steel	Tensile test	20 - 25
Jin et al [17]	TBC on Nickel superalloy	Tensile test	34 – 55

2.3 Coating Hardness

Adequate hardness is considered among the important properties that a coating is required to possess. As we introduced in the previous sections, hardness is defined as the resistance to plastic deformation induced by indentation or scratching. Despite the fact that scratch test, as it will be revealed in the next sections, can be used to calculate

hardness (scratch hardness), it has recently been used to define coating failures represented in terms of critical loads required to cause cracking, delamination, and coating spallation. Indentation is now the most common technique used to determine coating hardness. Usually, indentation is performed on the cross section of the coating to obtain a complete profile of the change of hardness with the distance from the interface, although indentation of the coating surface is of importance.

An interesting observation made by Culha et al [15], that the microhardness value decreases as the function of the distance from the coating surface deep into the coating material, and having the lowest values at the substrate surface interface, i.e hardness gradient from the coating surface to the interface. They used Carl Zeis micro-hardness tester, one of the Brinell hardness devices, for NiAl coatings on stainless steel substrate. In that study, they also investigated the effect of thermal cycling on the hardness for the same coating system. It has been reported that the thermal cycling reduces the hardness values without affecting the mentioned hardness gradient. However, a completely opposite trend was reported in the work of Eason et al [23], where for Cold sprayed copper coatings on hot pressed copper substrate, they showed that hardness is highest at the interface and starts to decrease. This is mainly due to the degree of cold working that takes place during the deposition process, which leads to an increased hardness in both, the deformed layer of the substrate as well as in within the spray deposit, i.e. hard substrate acts as a rigid impact, so the first layer of the coating that is in contact with the substrate will experience more deformation than the far away layers. A similar trend is reported in the work of Qian et al [24] where they studied the hardness relationship with the distance from the interface for Al-Si/Al_2O_3 prepared by laser plasma spraying. They

reported that the hardness is high at the interface and decreases gradually to the free end of the coating. According to them, this mainly because of the fact that the columnar crystal is dense close to the interface and decreases until it vanishes towards the end of the certain thickness, and that thickness, they studied, depends on the deposition parameter specifically the laser power. In the work of Sun et al [25], the micro-hardness of Fe-C-Cr-Nb-B-Mo coatings powder on different composition was examined in an attempt to increase the wear resistance for hardfacing applications. The coatings were prepared by laser cladding. Hardness was on the cross section, and no obvious trends were observed, rather, the values of the harness seemed to be constant throughout the thickness.

Table 2-2 Hardness values from the literature.

Author	Coating - Substrate	Test Method	Hardness Value
Koivuluoto and Vuoristo [12]	Cu+Al_2O_3 composite coating on Steel substrate	HV	80 - 130
Eason et al [23]	copper coatings on hot pressed copper substrate	HV	80 - 150
Triantou et al [13]	Cu+Al_2O_3 composite coating on Aluminum Alloy	HV	160 - 180
Wensheng et al [18]	Cu-14Al-4.5Fe on steel substrate	HV	290 - 320
Qian et al [24]	CuSn8 + AlCuFeB composite coatings on mild steel	HV	150 - 250

Hardness of the metallic coating can be enhanced by adding ceramic particles to the coating material before deposition. Triantou et al [13] studied the effect of various alumina (Al_2O_3) content on the copper coating hardness and wear resistance. Alumina powder was blended with the copper and the mixture was coldly sprayed on Aluminum

alloy 2017 substrate. Coating Thicknesses more than 150 μm were obtained, and hardness measurements were conducted using Vickers indenter. 2 to 9 % higher hardness values for the composite coatings in comparison to that of pure copper were reported , similar results were reported by Koivuluoto and Vuoristo [12]. In the work of Wensheng et al [18], the effects of adding Cerium to Cu-14Al-4.5Fe (Aluminum bronze) coating on carbon steel substrate was studied. Using Vickers indenter with 4.9N load, they found that, by only adding 0.6% Ce to the copper alloy, the hardness improved by 8.9%. Guo et al [26] concluded the same result cold sprayed tin-bronze based composite coatings. Table 2-2 shows some of the hardness values found in the literature.

Finite element (FE) analysis has been used by many researchers to model the indentation process. FE is often employed to study the stress field around the indenter tip. Sun et al [27] used Finite element analysis to study the effect of coating thickness to the indentation depth ratio on the indentation response of the layered systems. They also studied the effect of the indenter tip geometry on the critical ration of thickness to tip. Based on the Finite element analysis, they came up with an empirical equation that relates the critical thickness to depth ration to the yield strength ratio and indenter tip radius. Bolshakov, Oliver, and Pharr [28] used finite element to study the effect of applied or residual stress on the indentation process. They showed how biaxial stress in the sample has a great effect on the amount of pileup formed around the hardness impression, which has a significant effect on the calculated hardness and modulus values. Moy et al [29] used finite element to verify results of a proposed analytical method that combines the indentation curve with the imprint geometry to identify the mechanical parameters. Xiao et al [30] investigated the mechanics of indentation induced coating

interfacial cracking and delamination in brittle thin coating substrate systems. Finite element modeling of indentation has extensively been used to study coating failures and stress characteristic of the coating surface ad bonding layer [5-10]. Finite element has also been used to simulate Nano-indentation process by considering an appropriate dimension of both the indenter and the sample [5], [10 – 20]. Researches have shown that finite element modeling of indentation can be one of the appropriate methods of evaluation hardness and mechanical properties of materials by comparing the results obtained from the model with experimental results [23], [46 - 50].

2.4 Scratch Resistance

Scratch test can be used for many purposes as far as coating systems are concerned. Many failure modes can be detected through the scratch test, however, scratch test was used originally used to measure coatings adhesion [49]. Beegan et al [50] for the first time used scratch test for copper coatings. Their mean goal was to measure the scratch hardness of 500nm copper film on a silicon substrate and compare it with hardness measured from nano-indentation. Vencl et al [20] examined the effectiveness of using the scratch test on the coating cross section to evaluate the bond strength by comparing these results with results of the standard tensile test for adhesion of thermal spray coatings. They confirmed that comparing the results of these two tests is questionable although a match in the general trend exists that a higher tensile implies a higher scratch bond strength. In the work of Barletta et al [51], progressive and constant load scratch modes were used to test the scratch resistance of a single and multi-layered composite coatings. Their composite coating consisted of metal pigments of Al-Mg 4.5% fillers in a modified phenyl-methyl silicone. Rockwell C indenter with three different diameters was used, and

the scratch grooves were examined by SEM to study the residual depth. They found that smaller diameter indenter causes earlier failure which has been attributed to the fact that sharper indenter severely stresses the sample because of the high contact pressure. Pile-up formation was also observed on the side of the scratch groove in all of the cases. They also studied the effect of the sliding speed and they concluded that increasing the sliding speed results in an increase of the coating ability to resist damage. Futami et al [52] studied the deformation and damage induced by scratch for copper-graphite composites. Up to 40% volume of copper content in the composite was studied. They discovered that copper content in the composite plays an important role in the overall scratch resistance by controlling the contact pressure. In the work of Roy et al [53] interfacial adhesion of SiCN thin film (40-100 nm) on Cu/Si substrates was studied using Nano-scratch test. They used standard Berkovich indenter to perform the scratch test with a maximum load 5 mN, scratch length of 0.5 mm, and scratch speed of 10 μm/s. With SEM examination of the scratch groove, they found that the film cracks and delaminates on both sides of the crack path, and therefore they were able to calculate the critical load that caused adhesion failure. They also studied the effect of the tip radius on the critical load and concluded that as the smaller the radius of the indenter tip, the lower the critical load. This can be ascribed to the fact that sharp indenter will penetrate more in the material than blunt indenter. This finding was confirmed in the work of Barletta et al [51], where three different indenter tip radius were studied, namely 100, 200, and 800 μm. According to their justification, shaper indenters impose high specific contact pressure, and therefore, failure occurs earlier. They also studied the effect of the sliding speed on the coating failure, and they found that higher scratch speeds allow coatings to withstand the action

of the sliding indenter with less damage on the coating surface, and thus, delayed failure i.e. high critical loads. Both of the scratch speed and indenter radius along with the loading rate are collectively studied by Randall et al [54] for several coating materials (TiN, W, Al, DLC and Au). They investigated 20, 50, 100, 500 µm indenter radii. Influence of the scratching speed was studied over the range of 2-10 mm/min, whereas the loading rate was studied over the range of 2-10 N/min for three different scratching speed. For the indenter tip radius, they confirmed the same findings of Barletta [51] and Roy [53], which signifies the importance of the indenter choice if a certain coating system is to be tested. However, their result for the critical speed contradicts with the results of Barletta et al [51], where they found that as we increase the scratch speed the critical load decreases, indicating faster failure. Additionally, they found that the critical loads values increase only slightly with the loading rate for fixed scratch speed and scratch length, and therefore they concluded that the change of the critical load with the scratch speed and the loading rate is highly influenced by the coating system under consideration and cannot be generalized. In the work of Culha et al [15] the scratch test was used to assess the adhesion of NiAl coatings on 316L stainless steel. The surface scratches were investigated by OM and SEM. Ghabchi et al [55] studied the damage mechanisms and cracking behavior of Wc-CoCr coating deposited by thermal spraying. The thickness of their coatings was 200 µm, which is close to our coating thickness. They highlighted three different damage mechanism for elasto-plastic materials: plowing, friction and fracture.

2.5 Research Objectives

As it appears from the literature review that there is a lot of work done on assessing hardness, adhesion, and scratch individually for several coating materials. However, a comprehensive study that investigates these mechanical properties (adhesion, hardness, and scratch) combined together for copper and copper alloys has not been reported. Therefore, in this work, a comprehensive study of mechanical properties of copper and copper alloys will be conducted. The output of this study can be later utilized for antibacterial coating applications and an optimization can be made between the antibacterial capabilities and coating quality expressed in terms of acceptable mechanical properties.

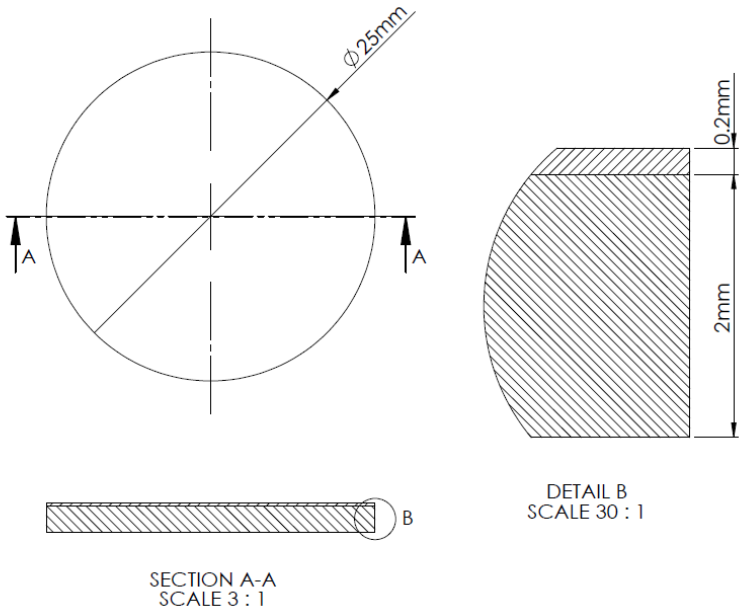

Figure 2-1 Shape and size of the samples

Coating materials to be studied in this work are listed in Table 1-1. All these coatings are deposited on stainless steel substrate disks of 25mm diameter as shown in

Figure 2-1. Three different thickness are available.

The following properties are to be evaluated and compared for different coatings and different coating thicknesses:

- Study of coating microstructure using SEM and XRD.
- Normal adhesion strength between coatings and substrate using pull-off adhesion tester (PosiTest AT-A 10285, DeFelsko Corporation), which measures the strength required to detach the coating perpendicular to the substrate surface.
- Coatings resistance to scratch using a scratch machine (Micro-Combi tester, CSM Instruments Corporation).
- Coatings hardness on the cross section (hardness profile) using Vickers micro-indentation test (Micro-Combi tester, CSM Instruments Corporation).
- The effect of changing coating structure and thickness on hardness, adhesion strength, and resistance to scratch.

CHAPTER 3

METHODOLOGY

3.1 Microstructure

Microstructure, morphologies, and elemental compositions of the samples were investigated using scanning electron microscopy (SEM). For each composition, two sets of samples were prepared for SEM examination, one for the top surface and the other for the cross section. Cross-section samples were prepared by diamond cutting with slow speed to avoid sample damage. Top surface samples were examined for studying the surface topography of coatings, whereas the cross-sectional samples were examined to investigate the coating properties, measure coatings thicknesses, and to study the interface between the coating and the substrate. Cross-sectional samples were slightly polished to ensure removal of residuals and damaged layers that might be introduced by cutting process. The SEM device used in this work was (JEOL MP-6113SNS) with a tungsten filament. The machine is also equipped with an EDS detector so that the elemental composition of the coatings can be estimated.

Phases identification and quantification were investigated using XRD. A diffractometer with Cu K_α (λ=1.54186 Å) was utilized. Scanning range was set to be10 to 100^o with a step of 0.02^o.

3.2 Surface Roughness

The roughness of the coating was measured by 3D profilometer. For each composition, three samples were taken and their surface roughness was measured. Measurements were done in such a way that a minimum of six measurements were conducted for every single sample to ensure the repeatability of the results.

3.3 Adhesion Strength

3.3.1 Pull-off Adhesion Test

This test method maximizes tensile stress from zero to the minimum stress required to detach the coating perpendicular to the substrate surface. So shear stress is not considered, and this is why results from this test cannot be compared to results obtained by other tests like scratch test or tape test.

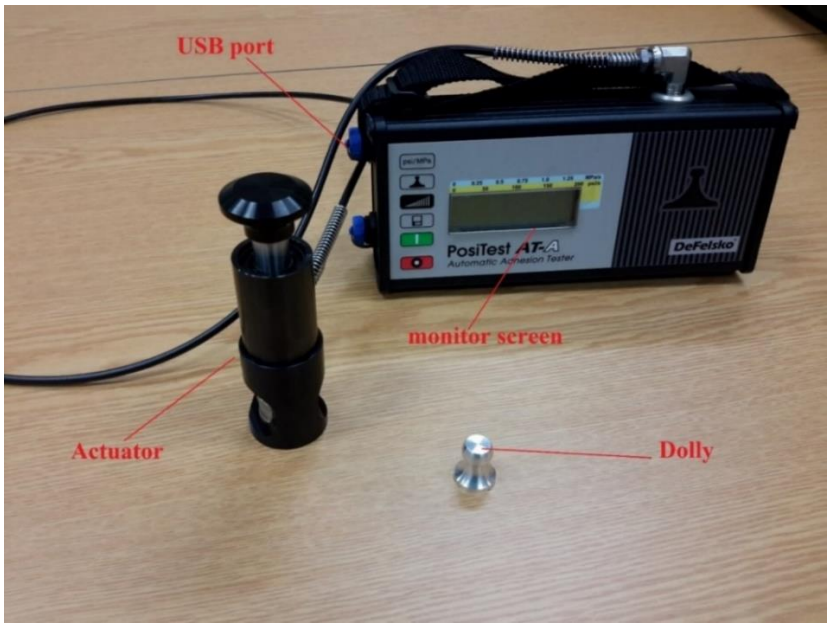

Figure 3-1 Pull-off adhesion tester components.

As shown in Figure 3-1, the major components of the pull-off tester are pressure source, actuator, and a pressure gage. The pressure source is simply a pump which can be operated manually or automatically depending on the type of the tester. Where the actuator is device responsible for grabbing and pulling the surface of the coating, and it is usually connected to the pump through a small pipe.

During the test, a loading fixture, commonly called stub or dolly, is glued to the coating surface by an adhesive, and when the adhesive has cured, a coupling connector is attached to the dolly. By activating the pump either manually or automatically, tensile stress is applied slowly to the actuator and the pressure gage provides a direct reading of the pull-off strength. Figure 3-2 illustrate the pull-off test mechanism.

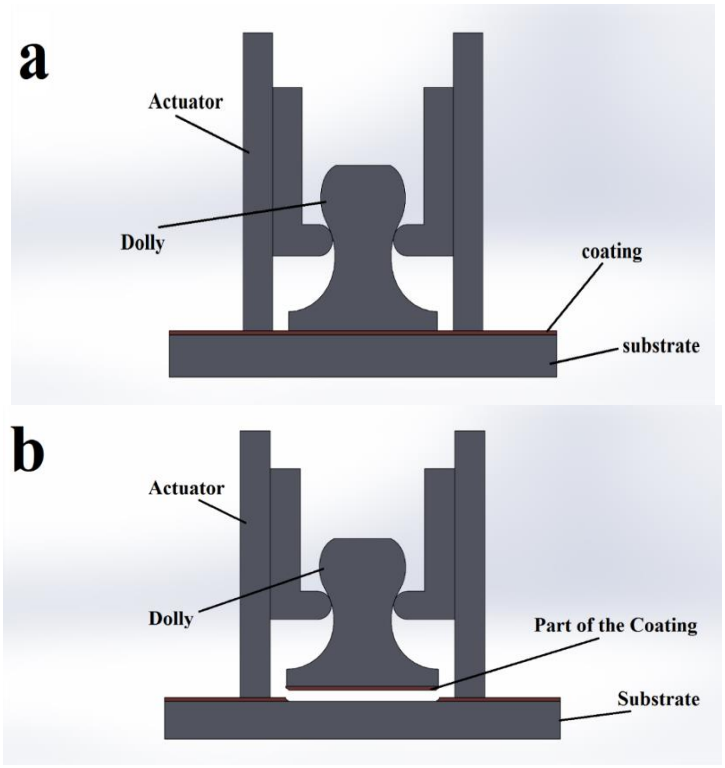

Figure 3-2 Actuator and the pulling process (a) before failure and (b) after failure.

3.3.2 Experimental Procedure

The dollies used in the experiment were disposable aluminum with 20 mm in diameter. First, the flat face of the dolly was degreased using a small soft tissue to ensure the removal of any traces of oils or grease. Then the dolly was abraded using an abrasive pad. The abrasion process was oriented for two purposes; to guarantee adequate bonding by increasing the available surface area, and to ensure the absent of any oxidation and rust. Then the surface of the dolly was cleaned to remove any particles especially those created by the previous abrasion process. The surface of the coating was also cleaned and lightly roughened.

Figure 3-3 Dolly applied to Cu sample after curing.

The adhesive used in these tests consisted of two-part epoxies. The adhesive was mixed and a uniform film of it was applied to the base of the dolly. Then the surface of the dolly at which the adhesive is applied was attached to the coating surface and the dolly was pushed down to squeeze out the excess adhesive. As per manufacturer's instructions, the

adhesive was left for 3 days to guarantee full curing. Figure 3-3 shows the dolly adhered to the sample after curing of the adhesive.

The actuator was connected to the head of the dolly through the quick coupling part, and full engagement of the dolly head was ensured. The device was powered-up and the displayed measurement units (MPa), dolly size (20mm) and pull rate (0.4 MPa) were verified. Then the test was initiated and the tensile stress started to build-up from zero MPa with a 0.4MPa increment, until it stopped when the dolly was completely detached from the surface, then the device was turned off.

3.4 Coating Hardness

3.4.1 Microindentation Test

Microindentation test was chosen because it is capable of detecting small changes in hardness values. Coatings hardness was measured using an instrumented microindentation machine (Micro-Combi tester, CSM Instruments Corporation), shown in Figure 3-4, with Vickers indenter. In micro-indentation, either the displacement (penetration) or the force can be controlled and the force-penetration curve is deduced from the experiment. In our work, we used force controlled indentation with applied force of Forces of 1N. It has to be noted that Vickers hardness values are independent of the force applied, this is mainly because the shape of the indentation is geometrically similar at all test loads as long as the test sample is reasonably homogeneous and force applied is big enough to avoid “indentation size effect” [56].

Indentation test cycle consists of two parts: loading and unloading. In the loading cycle, the load is applied gradually from zero up to the maximum load specified to the machine

at which the indenter reaches the maximum penetration. The indenter is then held at that particular depth (at maximum force) for 10 seconds (dwelling time). This is usually done to allow creep and time dependent plasticity to diminish. During unloading part, the indenter is retracted to a position of 10% of the maximum force where it is held for 30-60 seconds to measure the thermal drift of the machine, then the indenter is completely unloaded to zero force position in 2 seconds. Holding time (dwelling) depends on sample material and it is usually chosen such that the sample is not affected by creep. A wide range of holding times for different materials is suggested in the work of [57]. Usually, unloading rate is higher than loading rate in order to minimize the effect of thermal drift and creep.[58]

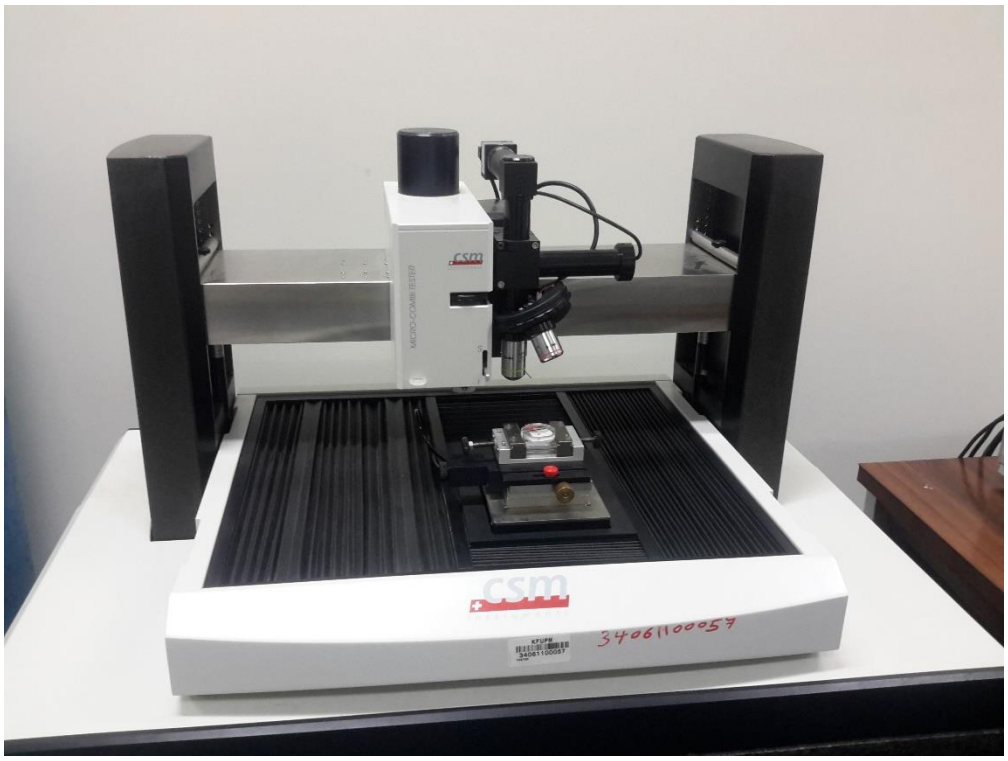

Figure 3-4 CSM Micro-Indentation machine

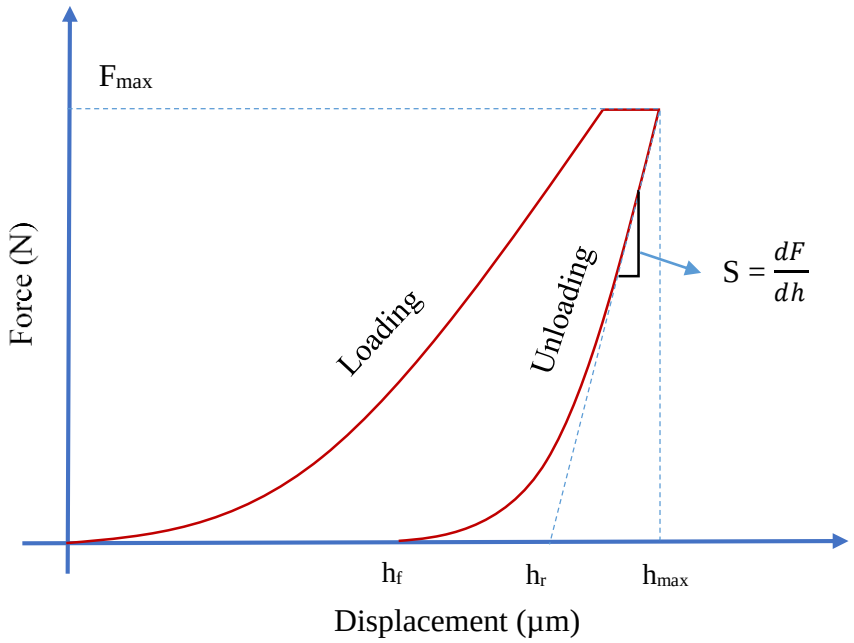

Figure 3-5 Typical Force-Penetration curve of indentation experiment.

Force-penetration curve is extracted from the experiment from which, hardness value can be calculated. Typical Force-Penetration curve is shown in Figure 3-5. Indentation is a powerful technique because only from the Force- penetration curve, hardness value and other mechanical properties such as Young's modulus can be obtained.

3.4.2 Hardness and Young's Modulus Calculation: Oliver & Pharr Theory

To calculate hardness and the elastic modulus of a material, the area of contact between the specimen and the indenter is required. Contact area can be calculated from the contact depth h_c and indenter geometry. Oliver & Pharr [59] proposed a mathematical model through which the contact area and thus the hardness can be calculated from the force-displacement curve. Their method suggests that the upper portion of the unloading curve in the force-penetration diagram can be fit into the following power law:

$$F = C\ (h\ -\ h_f)^m$$

Where F is the force, h_f is the final or plastic depth, h is the depth, C and m are constants.

Now, this curve is differentiated with respect to the depth h and evaluated at the maximum depth h_{max} to obtain the slope of the unloading curve, which is the stiffness of the material, i.e:

$$s = \frac{dF}{dh}\,(h = h_{\max}) = mC(h - h_{\mathrm{f}})^{m-1}$$

The contact depth h_c is then calculated from:

$$h_c = h_{max} - \varepsilon \frac{F_{max}}{S}$$

Where ε is a constant that depends on the indenter geometry. ε is 0.75 for Vickers and Berkovich indenter. Having the contact depth estimated, the projected contact area can now be calculated, by evaluating an empirically determined indenter shape function f, through:

$$A = f(h_c)$$

The indenter shape function basically relates the indenter cross-sectional area to the distance from the tip. For perfect Berkovich and Vickers indenters, the shape function is given by $f = 24.56\, d^2$, therefore, the contact area is:

$$A = 24.56\, h_c^2$$

Hardness can now be calculated as:

$$H = \frac{F_{max}}{24.56\, h_c^2}$$

The effective elastic modulus E_{eff} can also be calculated from:

$$E_{eff} = \frac{1}{\beta}\frac{\sqrt{\pi}}{2}\frac{S}{\sqrt{A}}$$

Where β is constant which depends on the indenter geometry. The effective elastic modulus is calculated with assumption that the elastic deformation actually occurs in the specimen as well as in the indenter. Therefore, the Young's modulus of the specimen can be from the effective modulus as follows:

$$E_{eff} = \frac{1 - v^2}{E} + \frac{1 - v_i^2}{E_i}$$

Where $E\ and\ v$ are the elastic modulus and Poisson's ration of the specimen, whereas E_i and v_i are the elastic modulus and Poisson's ration of the indenter.

3.4.3 Experiments

Micro-indentation tests were performed on the top surface of the coating as well as on the cross section. On the top surface of the coating, nine indents were made for each sample and the average values were considered. Indentations on the top of the coatings were performed without grinding or polishing the sample. This was mainly meant to avoid introducing changes to the microstructure of the coating through polishing or grinding.

For cross section indentation, samples were first sectioned using a diamond cutter with slow speeds. Samples were then epoxy mounted and the cross sections of the cut samples were thoroughly prepared by standard metallographic techniques such as grinding and polishing. Indentation was performed on the cross section of the samples to calculate hardness of the coatings as well as to study the effect of the distance from the interface to the surface of the coating on the hardness values. This is because thermally sprayed coatings exhibit different working hardening and residual stresses at different locations throughout the thickness. At each distance from the interface, a minimum number of 5 indents were made and 3 to 5 total distances were considered depending on total coating

thickness of the sample under consideration. Figure 3-6 illustrates how indentations were performed.

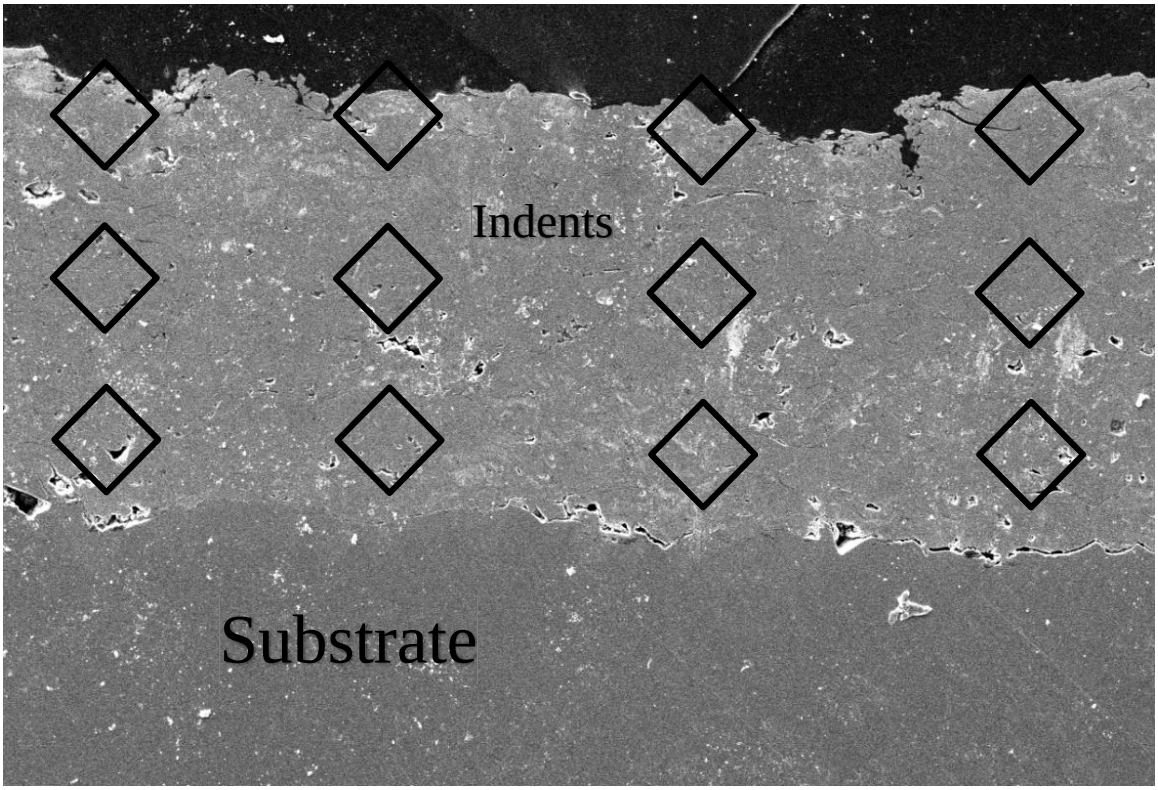

Figure 3-6 Indentation on the coating cross-section

3.5 Scratch Test

Scratch test measures coatings ability to resist scratch, cracking, and can also be used to measure coating adhesion to the surface of the substrate. It is also used to measure the scratch hardness. During scratch testing, as illustrated in Figure 3-7, an indenter or stylus of defined geometry, usually made of diamond, is drawn across the surface of the coating. The stylus moves with a defined normal force over a defined scratch length. The force can be constant, progressive, or it may increase incrementally. The stylus typically

has a spherical tip radius of 200µm. Depending on the load range, scratch test can be categorized into Nano-scratch, micro-scratch, and scratch.

Typically, micro-scratch is done in three steps: First, the indenter moves across the sample surface with a very low load to record the surface profile (this process is called pre-scan). Subsequently, the stylus contact geometry penetrates the surface of the coating and moves a constant speed until the end of the scratch length. Finally, post-scan is performed over the scratch groove at low load to measure the change in the morphology of the coating caused by the elastic recovery. Post scan enables us to determine the residual depth which is important for materials subjected to viscoelastic relaxation [51]. The tangential and normal forces, the penetration depth, and the acoustic emission signals are recorded continuously during scratch test.

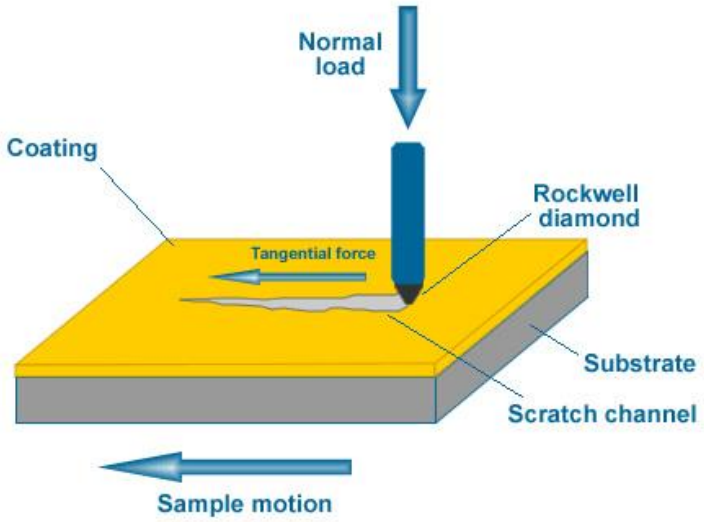

Figure 3-7 Schematic of scratch test

Usually, the scratch groove is analyzed using SEM or optical microscope (OM) to establish a well-defined failure damage such as deformation, cracking, spallation, delamination, or buckling. Accordingly, the critical load L_C is defined as the load

required to introduce a specific failure event (cracking, spallation, etc.). Many factors dictate the value of the critical load including the loading rate, the speed at the stylus moves, and the geometry of the stylus. Other parameters that also influence the value of the critical load are coating thickness, microstructure and roughness of the coating, hardness, Young's modulus, and fracture strength of the coating material [51][60].

Progressive scratch test

In this mode of the scratch test, the stylus moves across the surface of the coating with an increasing normal load to a maximum predetermined value. The normal force usually increases manually. The critical load is indicated as the normal force at which specific failure is first detected. Progressive load scratch test PLST is usually used, as per EN1071 recommendations, to assess the critical loads that correspond to major coating failures.

Constant load Scratch test

In this type of scratch test, the normal force is fixed at a constant level throughout the scratching process. Several scratches are made with different loads and studied to conclude the critical load of the coating corresponding to a specific type of failure. Constant load scratch test CLST mode allows statistical analysis of the damage of coatings along their interfaces.

Multi-pass scratch Test

This test mode is simply conducted by scratching the same groove more than one time. Loads used in the multi-pass scratch test are usually constant, and the operation parameters are usually the same as in the constant load scratch test mode. Number of the scratches until failure occurs is determined. The load used in multi-pass scratch is usually 50% of the critical load determined by progressive test mode. Multi-pass scratch test

mode represents a low cycle fatigue type of load for the coatings, and thus, it is considered to better simulate the real working circumstances encountered by most of the coated parts in service.

Experiment

Scratch tests were performed using scratch tester (Micro-Combi tester, CSM Instruments Corporation). Scratch tests were performed in two stages; first with a constant load to determine the scratch hardness, and secondly, with a progressive load to determine the failure behavior of the studied alloys. The indenter used in the tests using a Rounded Conical Rockwell C diamond indenter with a tip radius of 100µm.

In the constant load scratch test, the load was set to 20N for all sample. The Scratch length was 8 mm and the scratch speed of 5mm/min. Two scratches were made, and the average value of the width is recorded. The width, w, of the scratch groove is determined through optical microscope, and the scratch hardness can be calculated from the following equation [50]:

$$HS = \frac{8\,F}{\pi\,w^2}$$

Where F is the applied force.

In the progressive load scratch test, the load is set to increase linearly from 0.03N as preload to a maximum load of 30N. The Scratch length was set to 10 mm and the scratch speed of 5mm/min. Normal force, frictional force, penetration depth and the Acoustic emission were recorded throughout the scratch process along with images of the scratch grooves. Three scratches were made, and average values are considered.

3.6 FE Modelling of Microindentation

Micro-indentation process was simulated using commercial software ABAQUS with nonlinear elastic-plastic behavior of the coating material. A conical indenter that has half-angle of 70.3^{o} to have a same projected area to depth function as Vickers indenter was considered in the model as illustrated in Figure 3-8. The indenter was given elastic properties of diamond (Young's modulus of 1150 GPa and Poisson's ration of 0.1).

A 2-D axisymmetric model was utilized in the model. Insignificant difference between the results obtained by 3-D and that obtained by 2-D axisymmetric model is reported in [39]. The coating materials were assigned elastic/plastic responses with Kinematic hardening and the indentation was considered to be performed at room temperature. Young's modulus and Poisson's ratio values were taken directly from the micro-indentation experiments. Yield strengths are changed until the force penetration curves resulted from the experiments match the force penetration curve produced by the FE model.

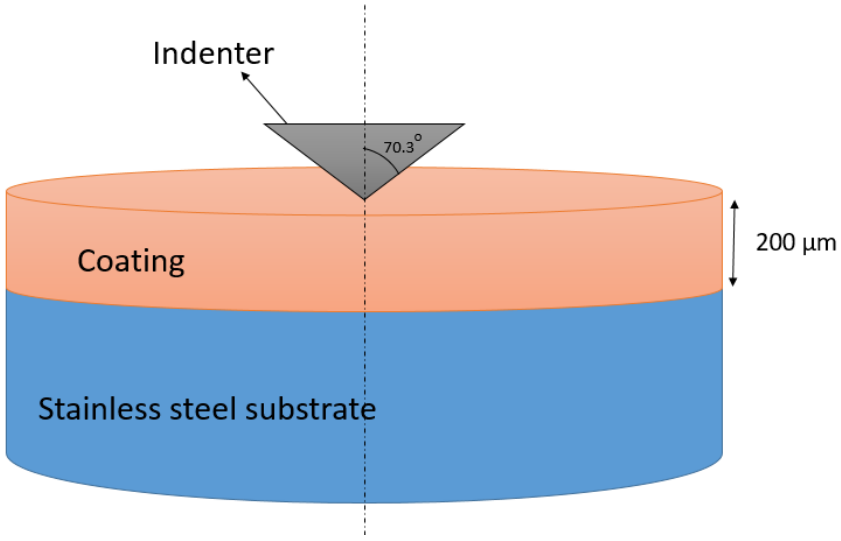

Figure 3-8 Schematic drawing of the coating system and the indenter.

Samples were modeled with four-node quadrilateral axisymmetric reduced integration elements. Refined mesh was used in coating corners immediately under the indenter tip and the coarse mesh far away, as shown in Figure 3-9. Mesh convergence was checked. As reported in [39], plastic deformation in the substrate at the interface zone will not be initiated unless the penetration depth of the indenter exceeds 15% of the coating thickness. In our case, the penetration depth (5 - 9 μm) was smaller than 10% of the coating thickness, so the substrate was not included in the model to reduce the computational time. Surface to surface contact was defined between the indenter and the coating surface with the indenter being the master surface, and because only the master surface can penetrate into the slave surface, the contact direction was defined from the indenter surface towards the coating surface. Boundary conditions were created to fix the coating systems from the bottom and to prevent the movement of the centerline in the x-direction.

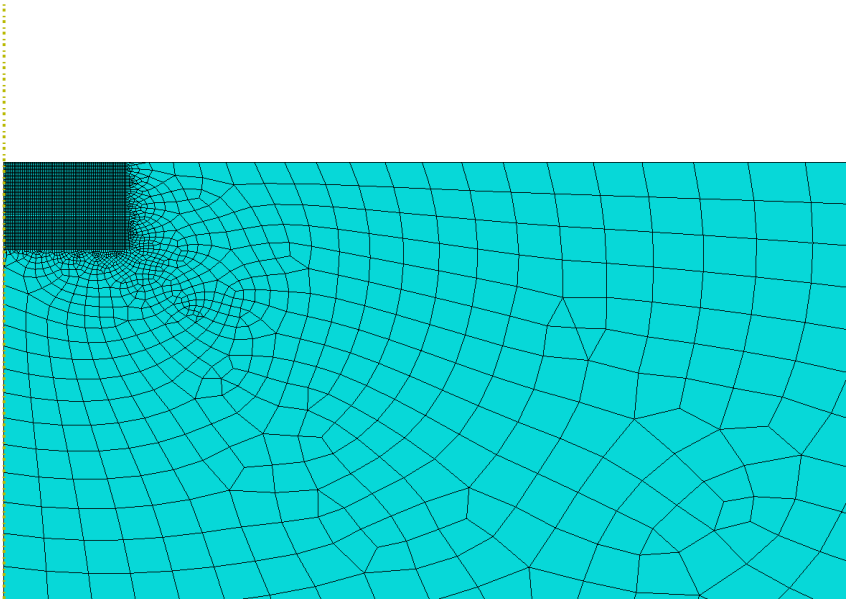

Figure 3-9 FE model mesh.

Two steps were created to simulate the indenter movements during loading and unloading. The first step was performed to enable the indenter to move a specific displacement (penetration) in –y direction (loading part) while the second step enables the indenter to go back to its initial position (unloading part). For pure copper coating, a displacement (penetration) of 8.7 μm was applied, whereas for Copper-Tin, Copper-Nickel-Zinc (German silver), and Copper-Aluminum-Iron (Aluminum Bronze), displacements of 7.93, 7.88, and 5.465 μm were applied respectively. These values are the averages of the penetrations reached in the experiments.

The main purpose of the FE models is to study the stresses under the indenter as well as to calculate the values of the yield strength and stress-strain curve of these alloys. This shall be done by changing the Yield strengths inputs in the model until the force penetration curves of experiments and that produced by the FE model match (Calibration). Having that achieved, values of stresses and strains are now taken from the model and considered as the material response. This is motivated by the fact that, although these alloys are common and their material properties are well studied, having gone through thermal spraying process would have changed their mechanical response to loads, and therefore, finding the mechanical response of these materials is of importance.

CHAPTER 4

RESULTS AND DISCUSSION

4.1 Coating Characterization

4.1.1 Chemical Compositions

Figure 4-1 shows some of the elemental composition analysis results. The elemental composition analysis using EDS was conducted for three samples for each alloy. For pure copper samples, traces of Si and Mn were detected. These elements may probably have diffused from the substrate (316L stainless steel) during deposition processes. Copper-tin alloy samples were found to have 4% of tin, Copper-aluminum-iron (Aluminum Bronze) samples contain 17%Aluminum and 1%Iron whereas copper-nickel-zinc (German Silvers) samples contain 17%Nickel 10%Zinc. No obvious variation of composition with the coating thickness was observed during for Copper-aluminum-iron (Aluminum Bronze) and copper-nickel-zinc (German Silvers) alloys, and almost all the samples with different composition reported close values of the elemental concentration.

As EDS analysis revealed, oxygen and carbon contents were found in all samples. These elements are commonly detected during EDS examination for all samples. It is also possible that these coatings contain some oxide, which is often the case with the thermal spraying of metals because of the fact that these processes are performed by melting the coating particles which result in their oxidation [7][61]. The oxide content depends on the spraying technique and the spraying parameters. These oxides are usually brittle and

therefore can reduce both ductility and strength of the coating [16-17]. However, metal oxides have been showed to improve some properties such as wear resistance [62].

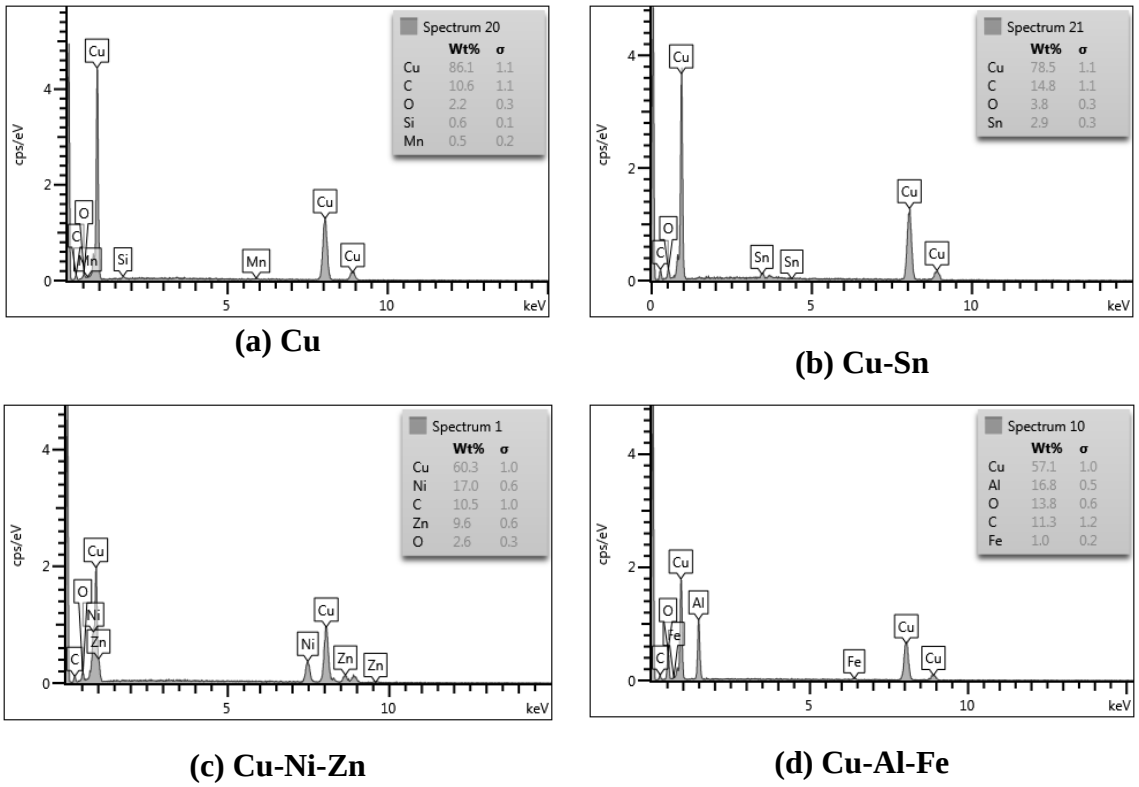

(a) Cu **(b) Cu-Sn**

(c) Cu-Ni-Zn **(d) Cu-Al-Fe**

Figure 4-1 EDS Spectra.

4.1.2 Microstructure and Surface Morphology

Figure 4-2 and Figure 4-3 show top view SEM micrographs of the samples at different magnifications. It can be observed from these images that the roughness of these coatings is extremely high, which is usually the case for thermally sprayed copper coatings [7][64], since the coating layer is formed through the impact of high velocity droplets on the substrate surface, and therefore it is impossible to obtain an even surface. Coating splats can be seen clearly from the images, and their size could be estimated to be around 80 to 120 μm in diameter.

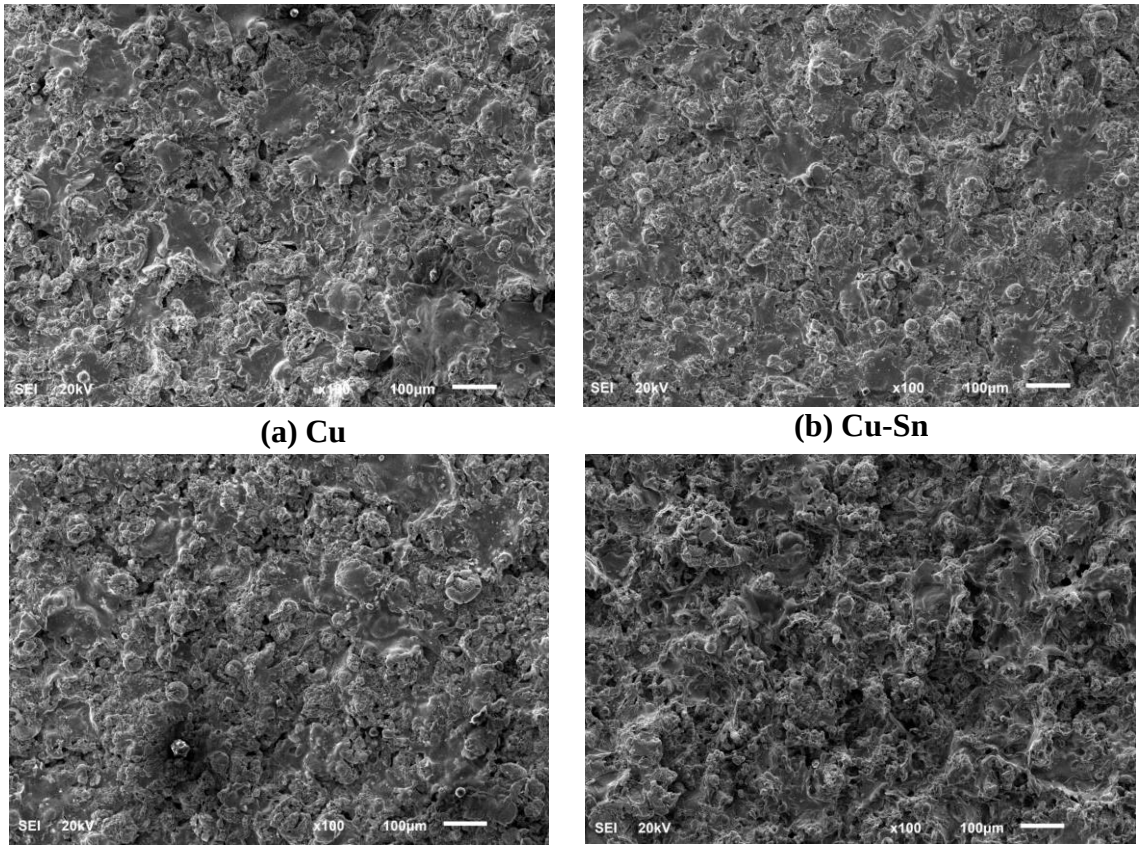

(a) Cu **(b) Cu-Sn**

(c) Cu-Ni-Zn **(d) Cu-Al-Fe**

Figure 4-2 Mx100 Top View SEM micrographs.

Pores can be detected from Figure 4-3 between the coating splats. This is usually because the metallic thermally sprayed coating splats have between them distinct boundaries and they usually tend to keep their individuality which allows the pores to grow inside the coating structure. similar observations are reported in [7] for pure copper coatings. Cu 17%Ni 10%Zn and Cu 4%Sn coatings also showed the same behaviors. Pores in coatings sometimes allow the penetration of oxygen, which may result in oxidizing the coating inside.

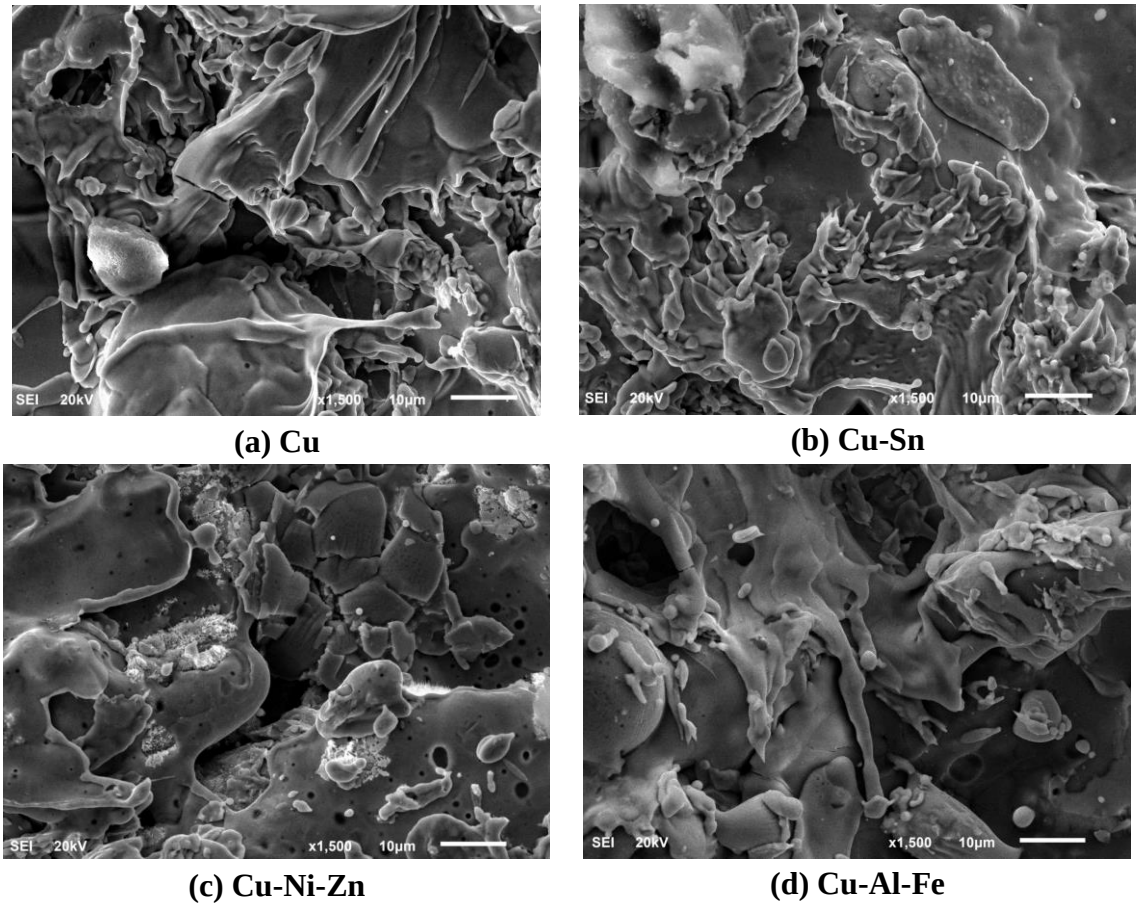

(a) Cu **(b) Cu-Sn**

(c) Cu-Ni-Zn **(d) Cu-Al-Fe**

Figure 4-3 Mx1500 Top view SEM micrographs.

Figure 4-4 shows cross-sectional micrographs of the tested samples. Pure copper samples were found to have a uniform interface. However, both cracks and pores can clearly be seen within the coating layer indicating relatively poor cohesion between the coating splats. For copper-tin samples, the coating appears to be weakly bonded to the substrate surface. Nevertheless, copper tin coatings showed relatively fewer pores compared to pure copper. This may be due to the fact that thermally sprayed tin coatings, as reported in [65], tend to form splats with integrity, and hence, having tin with copper in the alloy is expected to yield more integrate less porous coating surface.

Copper-nickel-zinc coatings showed high porosity as in the case of pure copper samples, and the interface for these alloys was found to be cracked indicating less adhesion to substrate. However, for samples with lower thickness, the interface was found to be more uniform and the coating seemed adhered to the substrate.

The interface in copper-aluminum-iron samples was observed to be almost flawless and the coating seemed adhered to the substrate surface. Another observation that can be made for copper-aluminum-iron samples is that the interface seemed to have experienced high deformation during deposition, indicating high bond strength. Copper-aluminum-iron coatings appeared also showed less porosity compared to other coatings.

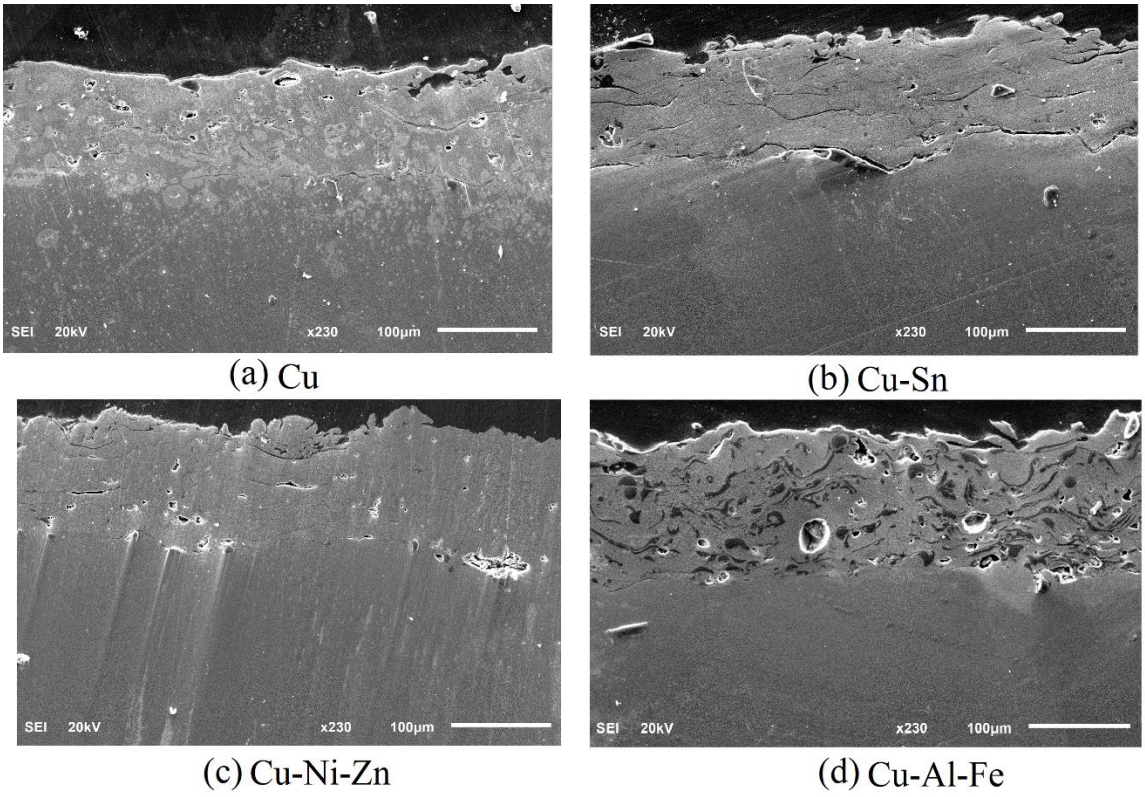

Figure 4-4 Cross Section SEM micrographs.

4.1.3 Phases Identification

Figure 4-5 Show the XRD spectra of the four different compositions over a 2θ range of 10 – 100°. It was found that only one phase is formed for each alloy, which indicates that neither secondary phases nor oxides are formed in these samples. Moreover, it can be observed that similar spectra, in terms of shape and number of peaks, were found for the four different compositions, and the only differences are the location and intensity of the peaks. This is may be due to the fact that all of these samples contain more than 70% of copper, and therefore their resulted spectra will be close to each other.

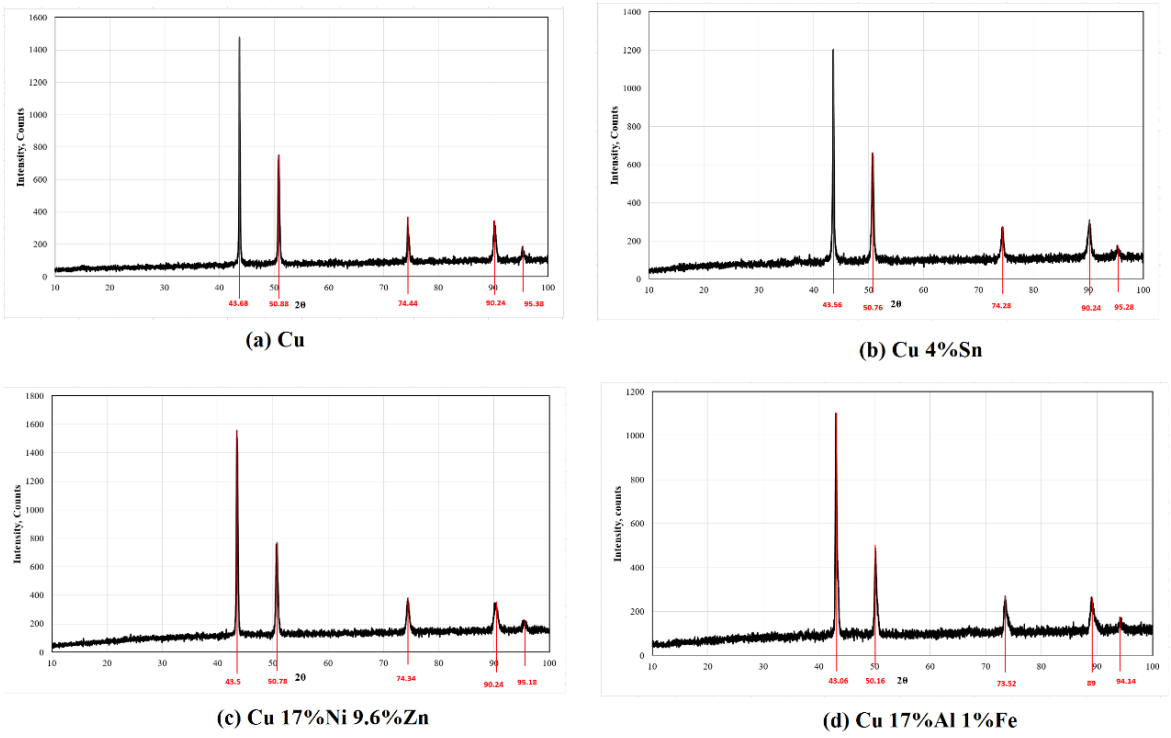

Figure 4-5 XRD spectra

4.2 Surface Roughness

Values of the surface roughness represented in terms of the arithmetic means (R_a) are listed in

Table **4-1**. In general, high values of roughness were found for all of the samples as it was anticipated from the SEM top surface micrographs. This is usually the case with thermal spraying processes, as discussed in the previous sections. When the molten particles hit the surface and form splats, possibilities of defects formation and non-uniform surface are high, which result in a surface with a high roughness. Surfaces become even rougher when a part of the molten particles partially or totally solidifies before reaching the surface of the substrate or the already formed coating. Among the tested composition, the lowest roughness was registered for Cu 4%Sn samples.

Table 4-1 Average Surface Roughness.

Coating Composition	Surface Roughness (Ra)
Cu	12 ± 1.59
Cu 4%Sn	10.85 ± 1.81
Cu 17%Al 1%Fe 150 µm	16.46 ± 1.98
Cu 17%Al 1%Fe 200 µm	15.61 ± 1.84
Cu 17%Al 1%Fe 300 µm	18 ± 1.72
Cu 17%Ni 10%Zn 150 µm	11.77 ± 1.16
Cu 17%Ni 10%Zn 200 µm	13.6 ± 1.9
Cu 17%Ni 10%Zn 400 µm	15 ± 2.1

Aluminum Bronze samples (Cu 17%Al 1%Fe) showed slightly higher roughness than the other compositions. Nevertheless, values of the arithmetic mean for these samples can said to be close to each other. This may be due the fact that the same deposition parameters are used for all samples. Figure 4-6 Shows typical 3D surface profile of these samples. Roughness of the coating surface may be desirable in some applications such as antibacterial coatings.

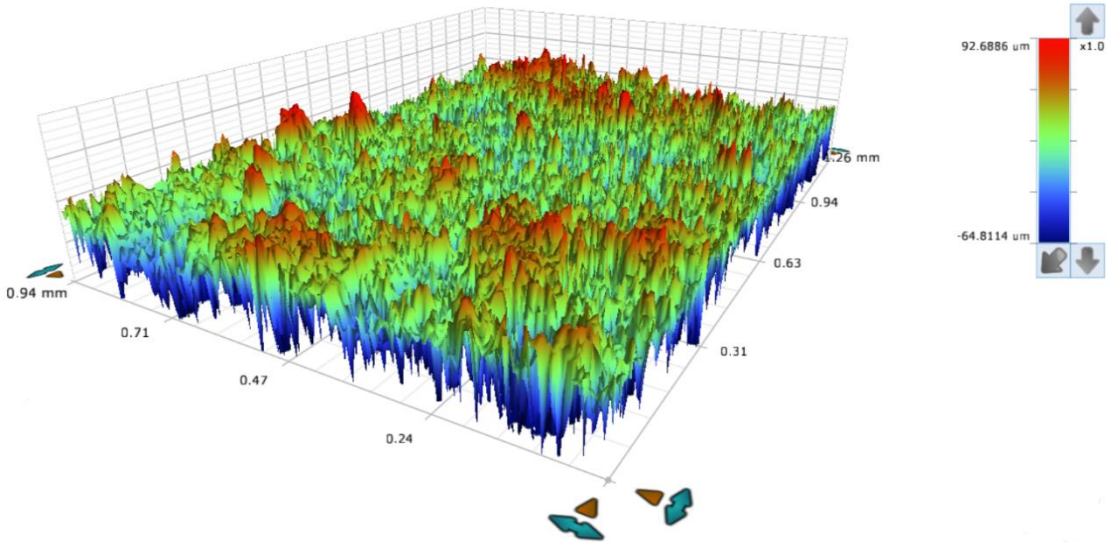

Figure 4-6 3D surface profile of a Cu sample.

4.3 Adhesion Strength

Figure 4-7 shows the coating before and after the pull-off test for a Cu sample. It can be seen that the coating completely detached from the substrate surface with the failure occurred evenly, and the part of the coating material that the dolly had adhered to, was removed completely from the substrate. Coating samples with different compositions and thicknesses showed the same total removal of the coating material from the adhesion test area except Cu 17%Al 1%Fe samples, which part of them did not fail. Average values of the adhesion pressure are shown in Table 4-2, as well as in Figure 4-8. It can be observed from Figure 4-8 that, Cu 17%Al 1%Fe samples have high adhesion strength, i.e. strongest interface, in fact, Cu 17%Al 1%Fe samples of 150 and 200µm did not fail at the interface, but at the adhesive layer between the coating and the dolly, indicating that the adhesion strength of these samples is higher than the epoxy glue strength. This may be attributed to the fact that Cu 17%Al 1%Fe samples had higher interface deformation

compared to other samples as revealed by SEM micrographs of the cross sections (Figure 4-4). Also, as reported in [11], Al bronze coating often undergoes metallurgical interaction during spraying process between the sprayed particles and steel substrate, often represented in the diffusion of the Fe into steel substrates or vice versa, giving rise to a high bonding strength.

Figure 4-7 Adhesion test on a Cu sample, (a) before, (b) after failure.

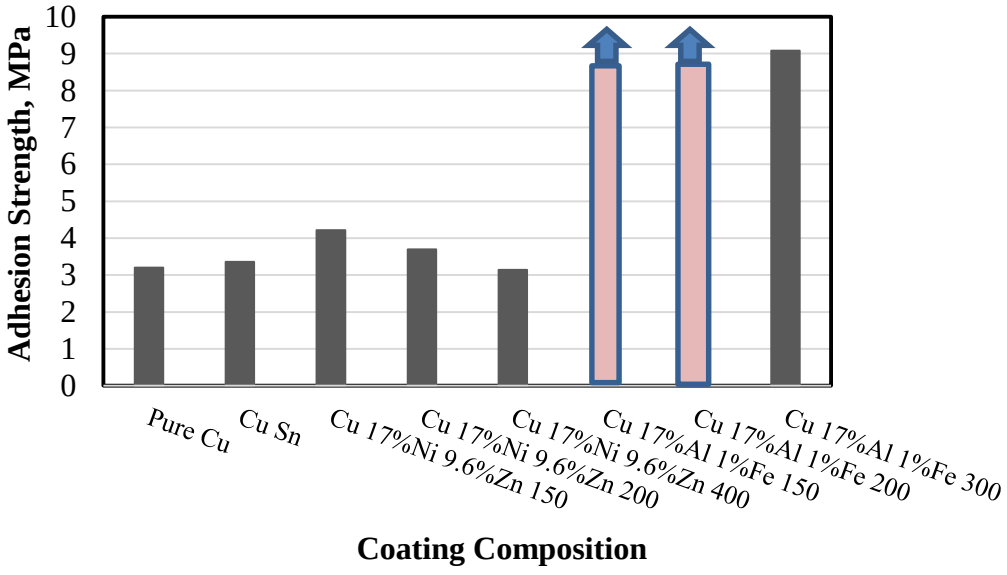

Figure 4-8 Pull-off adhesion strengths.

Table 4-2 Adhesion strength values

Coating composition	**Approximate thickness (microns)**	**Adhesion Strength (MPa)**		
		Sample 1	Sample 2	Av
Cu	150	3.24	3.17	3.205
Cu 4%Sn	150	3.47	3.25	3.36
Cu 17%Al 1%Fe1	150	NF	NF	NA
	200	NF	NF	NA
	300	9.08	NF	9.08
Cu 17%Ni 10%Zn	150	4.17	4.26	4.21
	200	3.62	3.78	3.70
	400	3.24	3.04	3.14

On the other hand, pure copper and Cu 4%Sn alloy samples were found to have the least adhesion strength, which may be attributed to the fact that for these samples, especially for Cu 4%Sn, some cracks were detected at the coating-substrate interface during the SEM examination. Therefore, the cracked interface assists the adhesion failure of these coatings.

Cracks at the interface were also detected for Cu 17%Ni 10%Zn samples of 200 and 400 µm. Accordingly, the adhesion strengths for these two particular thicknesses were found to be relatively low compared to the samples of the same composition but with 150 µm thickness where no cracks were observed at the interface as shown in Figure 4-9.

Figure 4-10 shows the variation of the adhesion strength with coating thickness for Cu 17%Ni 10%Zn coatings. As it can be observed from the figure that the adhesion strength decreases as the coating thickness increase. This can further be supported by the fact that for Cu 17%Al 1%Fe samples of lower thicknesses did not fail, although for the same

composition, samples of higher thickness failed. This is because residual stresses in thicker coatings are usually higher than that in thinner coatings, and therefore, more driving force for crack propagation at the interface is induced by the presence of these stresses. Similar observation for thermally sprayed metallic coating was reported in [66][67]. Another reason for the adhesion to decrease with the coating thickness is that a coating of higher thickness complies easily with the pulling action compared to lower coating thickness.

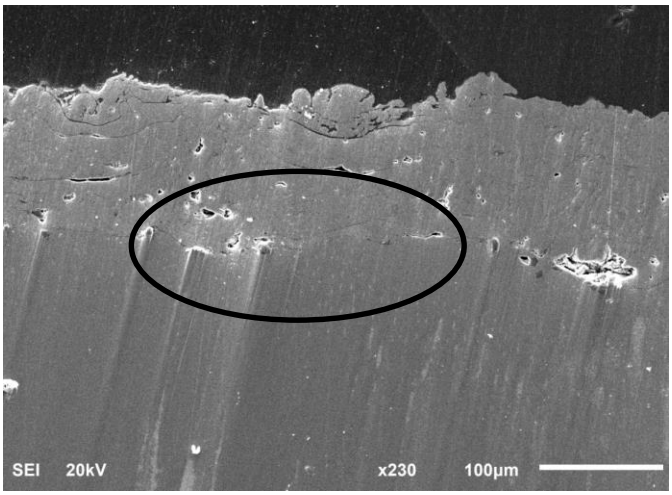

(c) Cu-Ni-Zn 150 µm

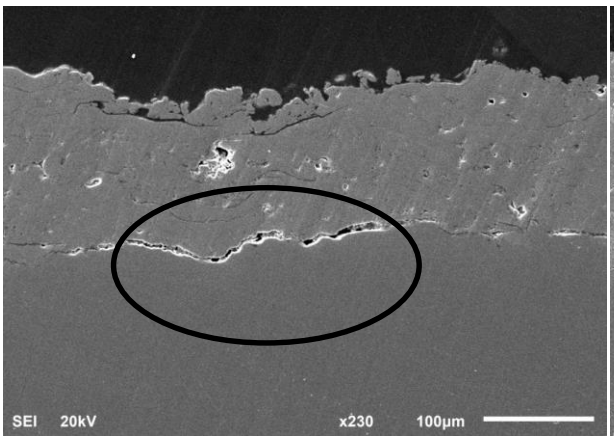

(a) Cu-Ni-Zn 200 µm

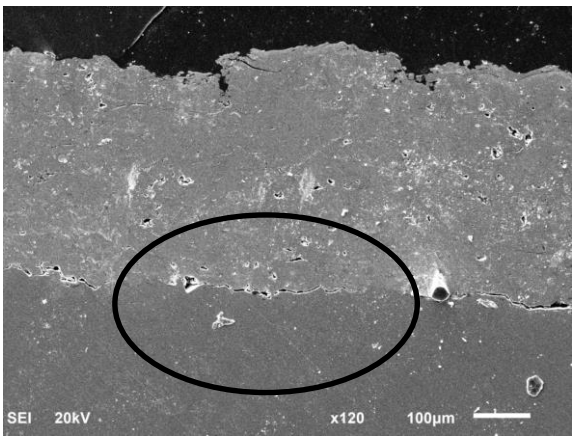

(b) Cu-Ni-Zn 400 µm

Figure 4-9 Interfaces of Copper-Nickel-Zinc samples.

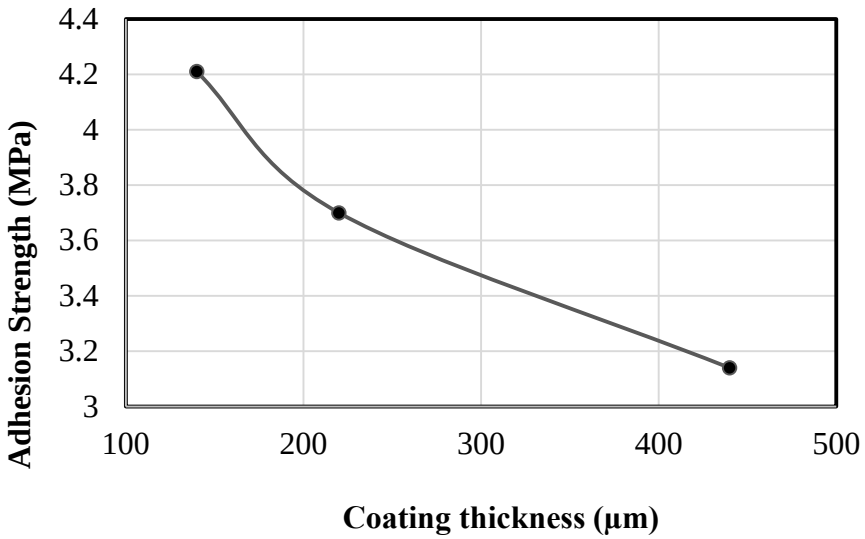

Figure 4-10 Effect of thickness on the adhesion strength of Cu 17%Ni 10%Zn samples.

4.4 Microindentation Results

4.4.1 Hardness on The Top Surface

Values of Vickers hardness of the top surfaces of the coatings are showed in Figure 4-11. In general, hardness on the top of the coating is lower than that obtained from the cross as it will be shown later. This may be due to the fact that some of the indentations might have been performed on a part of the coating material that lies on the top of the rough surface, where hardness is expected to be low compared to the part of the material that lies on the bottom surface. The error bar shown in Figure 4-11 reveals the variation of the hardness values. High variations of the hardness values were found for all samples. This is mainly due to high surface roughness and defects associated with thermal spraying as discussed in section 4.2., where the origins of load penetration curves, from which hardness is deduced, correspond to the contact of the indenter with a part of the coating that may be located at the top of the rough surface or at the bottom of it, which inevitably lead to the discrepancy of the results. Similar variation in Vickers hardness values of

thermally sprayed coatings was reported in the work of Chicot et al [68], where indentation was conducted on the top surface of unpolished samples.

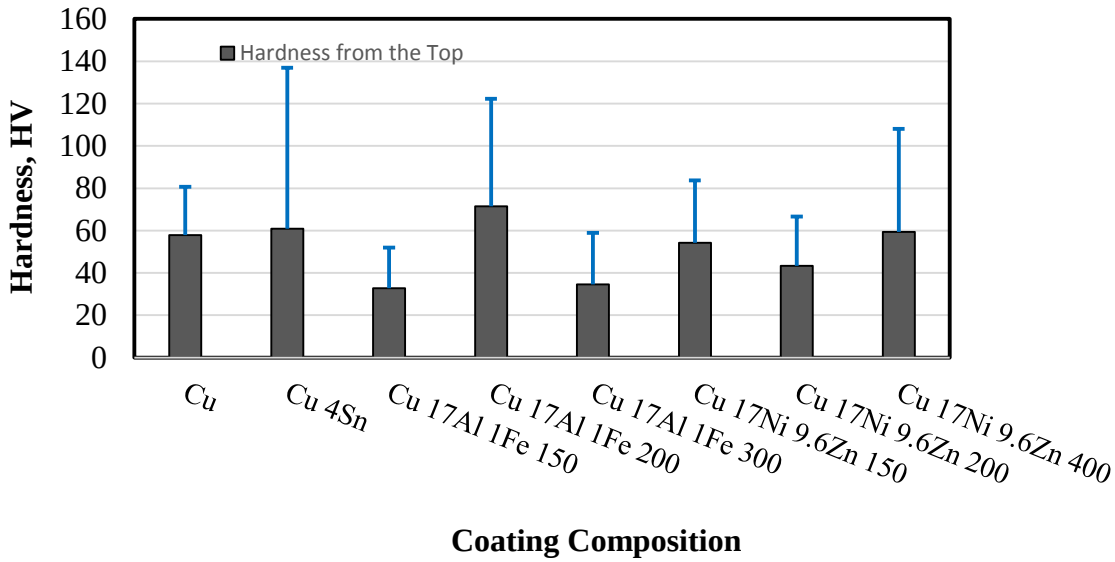

Figure 4-11 Hardness on the top surfaces.

4.4.2 Hardness Near The Interface

Figure 4-12 Shows the hardness values for the studied coating composition. The values displayed in the figure are evaluated at a point near the coating-substrate interface. It can be seen from Figure 4-12 that Cu 17%Al 1%Fe 300µm has the highest interface hardness, whereas Cu 17%Ni 10%Zn 200µm has the lowest. It has to be noted that the overall hardness of coatings cannot be judged by only measuring the interface hardness. This because many factors may contribute to the hardness of the coating at the interface including residual stresses and work hardening during the deposition process, and therefore, the rest of the coating thickness and top indentation have to be considered. Nevertheless, the Cu 17%Al 1%Fe samples, as it will be revealed in the next sections, showed high hardness at all position (top and cross section). This can be ascribed to the

relatively high content of the Aluminum in these alloys. usually, standards Cu-Al-Fe alloys are cast material and the percentage of the Al in the alloy is limited to 12% as maximum. Spray-forming enables incorporation of high aluminum content in the alloy, which in turns, increases the hardness and Young's modulus of the alloy substantially as investigated by Kudashov et al [10].

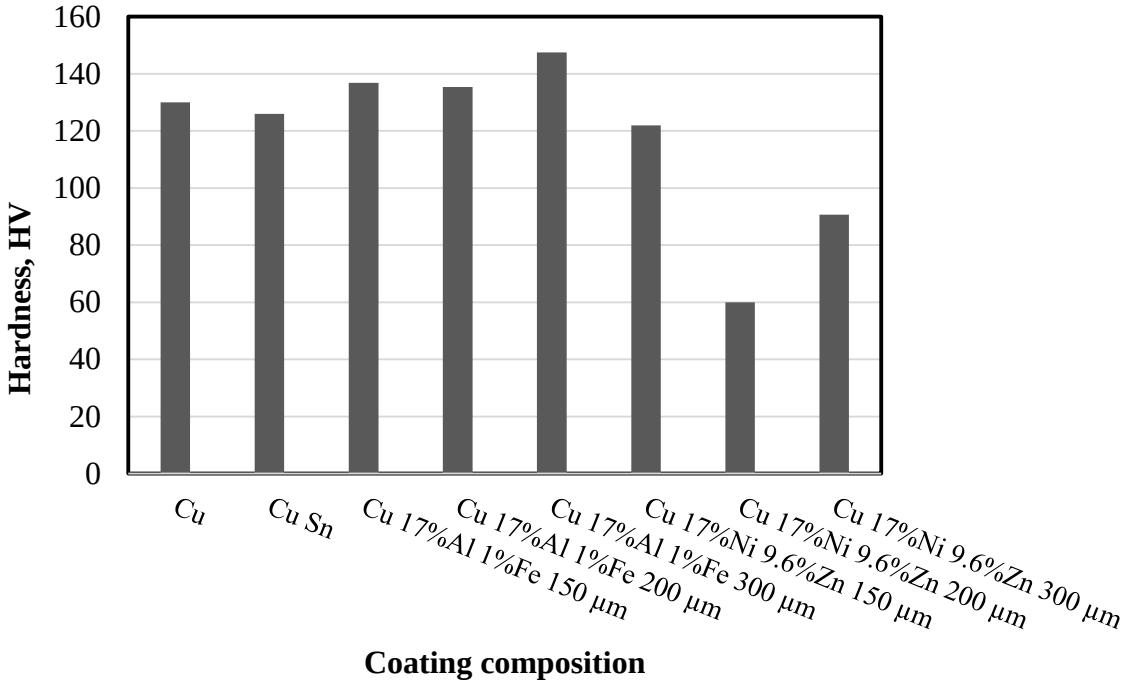

Figure 4-12 Coatings hardness near the interface.

4.4.3 Hardness Across The Coating Thickness

Figure 4-13 shows the variation of the hardness with the distance from the interface, where the exact location of the interface is at zero distance. As it can be observed, a general trend was found where hardness is high at locations close to the interface and then decreases with the distance from the interface towards the surface of the coating. This is because, during deposition process, the first coating layer near the substrate is

likely to experience more work hardening than the layers to come after especially if the substrate material is harder than the coating particles, which is the case of steel substrate, thus the substrate acts as a rigid impact for the coating particles. Molten particles that come after the first layer has been formed, are going to experience less impact hardening owing to the fact that they interact with a layer of a coating instead of the steel substrate. This claim is supported by similar findings in [23] for copper coatings.

Some of the samples were found to have low hardness values close to the interface. Figure 4-13 (c) shows the change of the hardness with the distance from the interface for Cu 17%Ni 10%Zn samples. Three different thicknesses of Cu 17%Ni 10%Zn samples are displayed, namely, 150, 200, and 300 µm. Near the interfaces, 150 µm coating showed the highest hardness compared to 200 and 300 µm coatings. However, hardness value of 150 µm coating samples drops rapidly with the distance from the interface and registers the lowest value at the end surface of the coating in a trend similar to that of the pure copper, and Copper-tin samples. Oddly, the highest values of HV hardness for 200 and 300 µm coatings samples were not at the interface, but 40-60 µm away. Near the interface, intermediate values of hardness were observed, then the hardness starts to increase with the distance from the interface until it reaches the highest values at 60 µm, then it starts to drop to its minimum values at end surface of the coating, so the trend looks as if the hardness values close to the interface were reduced. This can be regarded to the presence of the cracks that can be observed along the contact line (interface) between the coating and substrate as shown in Figure 4-9. These cracks at the interface may relieve the stresses that supposed to cause hardening of the layers in contacts with the substrate, and therefore reduce the hardness of that layer. This can be further

supported by the fact for the Cu 17%Ni 10%Zn samples of 150 µm where cracks were not observed at the interface, rather, the interface was found to be uniform, high hardness values were observed.

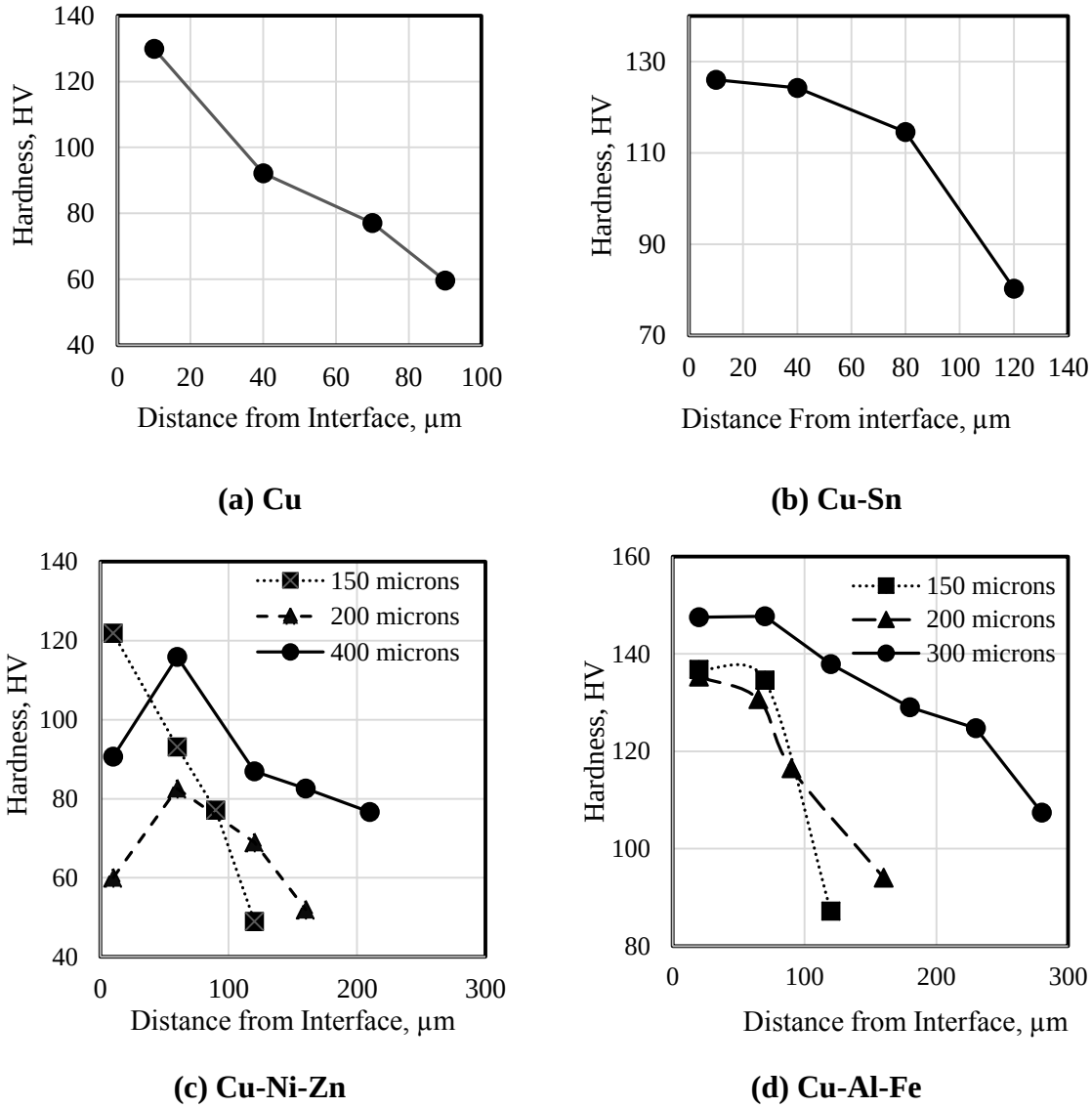

(a) Cu **(b) Cu-Sn**

(c) Cu-Ni-Zn **(d) Cu-Al-Fe**

Figure 4-13 Hardness profiles.

Hardness trends for Cu 17%Al 1%Fe samples are shown in Figure 4-13 (d). As mentioned earlier, Cu 17%Al 1%Fe coatings have relatively high hardness compared to other coatings mainly because of the high Aluminum content and the iron particles. For

this composition, the highest interface hardness was registered for 300 µm coating samples. Cu 17%Al 1%Fe of 150 µm and 200 µm showed a relatively close trend with their interface hardness almost identical. Cu 17%Al 1%Fe samples showed the same trend of the pure copper samples where the hardness is high at the interface, and decreases with the distance from the interface to the far end the coating surface, mainly because of the high stress and work hardening of the layers that are in contact with substrate, since no cracks were detected at the interface for this composition.

Another observation that can be made from Figure 4-13 (c) and (d), is that as the coating thickness considerably increases, hardness increases at most of the location across the coating thickness indicated by the fact the whole curve (hardness trend) was found to move upward with the thickness. This can be ascribed to the fact that residual stresses in thicker coatings are higher than that of thinner coatings especially the component of residual stresses caused by the thermal expansion mismatch between the coating and the substrate materials. This mismatch introduces compressive residual stress in the coating layer, and these stresses are intensified when the coating thickness increases, which in turn, increases the hardness of the coating.

4.5 Scratch Test Results

As mentioned in section 3.5 that two scratch tests were performed on these copper alloys; one with a constant load to determine the scratch hardness, and the other with a progressive scratch test to study scratch resistance for these alloys.

4.5.1 Scratch Hardness

Figure 4-14 shows an optical microscope picture for the scratch groove of Cu 4%Sn sample that illustrates how the scratch groove width was calculated. Values of the scratch groove widths along with the calculated scratch hardness are presented in Table 4-3. For better representation, the scratch hardness values further are plotted in Figure 4-15.

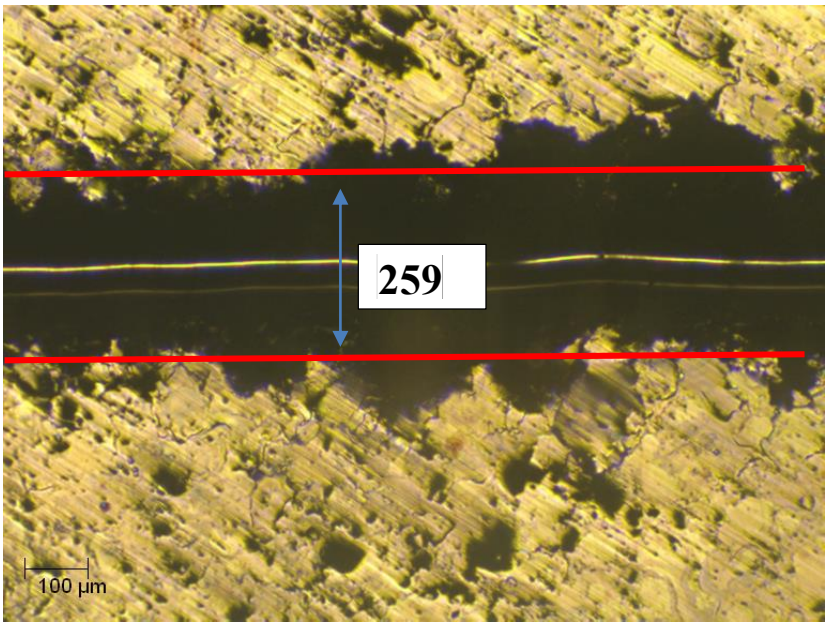

Figure 4-14 Scratch groove for a Cu-Sn sample.

Table 4-3 Scratch hardness values.

Coating composition	Thickness (µm)	Width 1 (µm)	Width 2 (µm)	Scratch Hardness (GPa)
Cu	150	266	271	0.70645
Cu 5%Sn	150	243	259	0.80839
Cu 17%Ni 10%Zn	150	299.4	291.18	0.58408
	200	275	281	0.65899
	400	250	254	0.80199
Cu 17%Al 1%Fe	150	252	255	0.79252
	200	248	235	0.87324
	300	215	218	1.0865

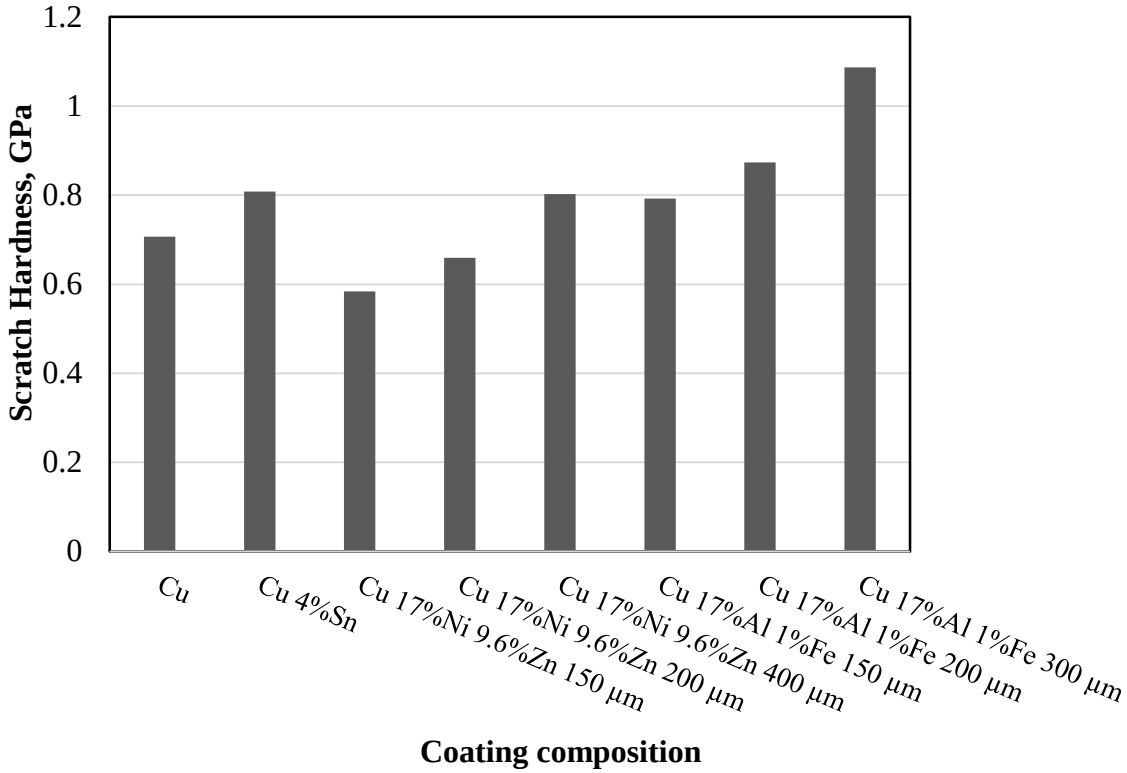

Figure 4-15 Scratch hardness values.

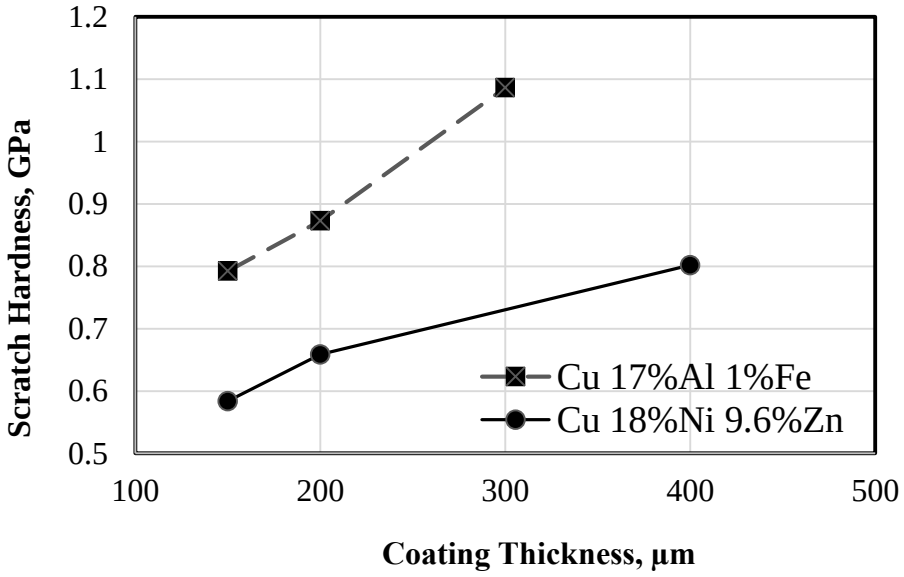

Figure 4-16 Effect of coating thickness on scratch hardness.

It can be seen from Figure 4-15 that, as in indentation, Cu 17%Al 1%Fe samples have the highest scratch hardness compared to other samples. This is may be due to the presence of the Fe and Al in the composition of this alloy, which makes it a little harder than the others.

Another observation that can be drawn from the scratch hardness results of these alloys is that, as far as the same coating composition is concerned, scratch hardness increases with the coating thickness as further illustrated in Figure 4-16. This can be attributed to the fact that higher thickness coatings are likely to have more closely packed splats than coatings with small thicknesses. Also, compressive residual stresses in thicker coatings are higher than that of thinner coating, which increases the hardness of the material as previously discussed in indentation hardness results. This is supported by indentation hardness results where indentation hardness was found to increase with the coating thickness (Figure 4-13) indicated by the fact that the curve of the hardness trend goes up with the coating thickness. A similar observation was reported in [69]. This observation is of great practical importance since it can be one of the methods to enhance the scratch hardness of an alloy because sometimes the amount of a certain element in the alloy can be limited to some reasons such as the solubility limit. For example, in the Aluminum bronze alloys, adding more aluminum to the alloy would improve scratch hardness of the alloy [10], however, the amount of the aluminum that can be added to the bronze is limited. Therefore, to increase the scratch hardness of the alloy, increasing the thickness may be a solution.

4.5.2 Scratch Behavior

Figure 4-17 shows the Force penetration curves of the tested samples. Figure 4-18 shows the depth reached for each sample at the maximum normal force. It can be observed that at the maximum force (30N) the coating has not completely been breached and the substrate has not been reached. Therefore, failure loads at which the coatings are delaminated cannot be found. Moreover, since these materials are ductile, they do not crack, and hence, the critical loads at which cracking starts cannot be identified either.

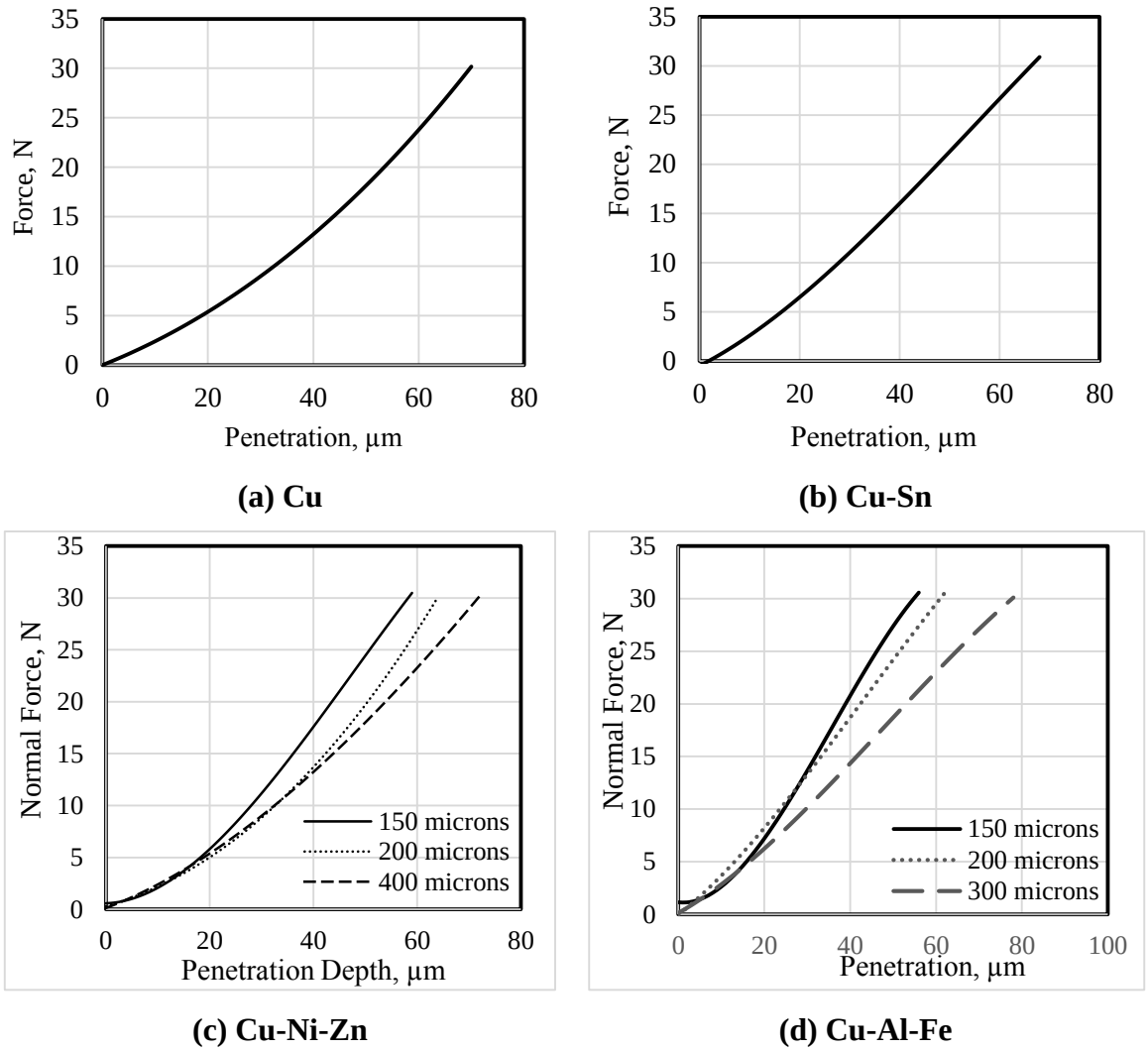

Figure 4-17 Scratch Force-penetration curves.

Nevertheless, we propose a method by which the scratch resistance of these samples can be compared, and that is to look at the force that produces a certain depth (depth that is fixed for all samples). We choose a depth of 50 µm as critical depth for all samples because 50 µm was reached in all samples. Now with that assumed, Figure 4-19 shows the forces at which a 50 depth is reached at each sample. It can be seen that Cu 17%Al 1%Fe samples have the highest scratch resistance, where higher loads are required to produce a scratch of 50 µm depth. This is again can be attributed to the fact that Aluminum hardens the bronze especially if it exits with a percentage of more than 12% as discussed in [10].

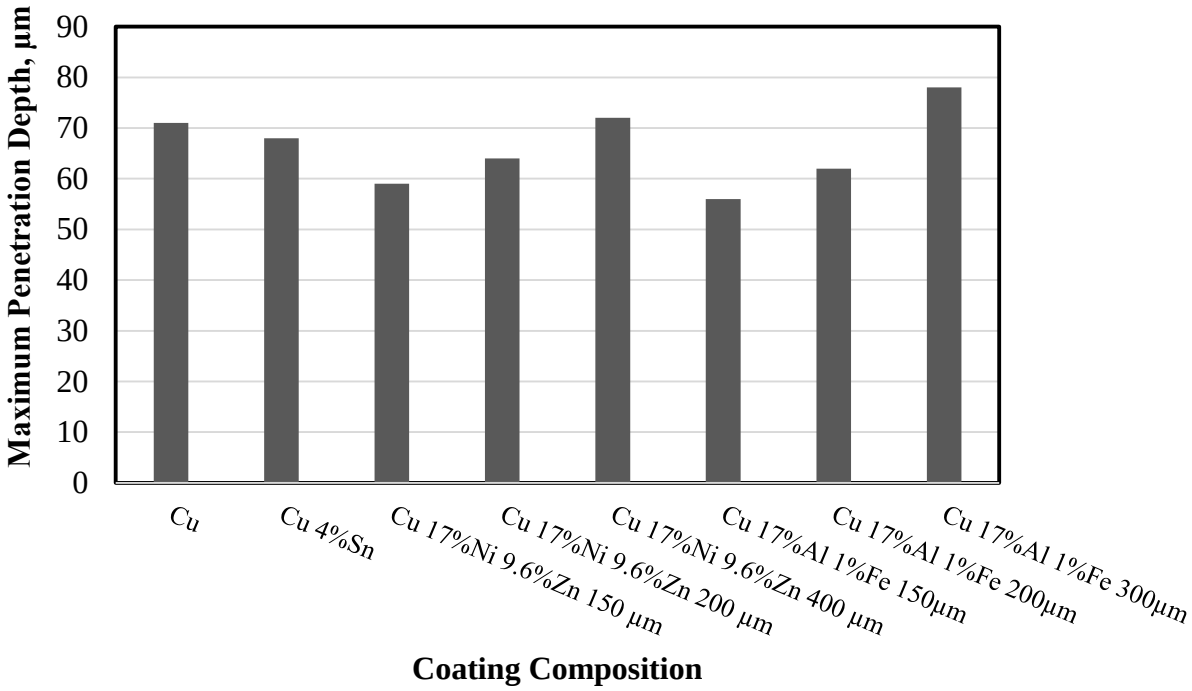

Figure 4-18 Maximum depths reached during scratch test.

It can also be observed that the scratch resistance decreases with the coating thickness for Cu 17%Ni 10%Zn and Cu 17%Al 1%Fe samples, indicated by the fact that lower loads are required to penetrate the higher thickness samples up to a penetration depth of 50µm.

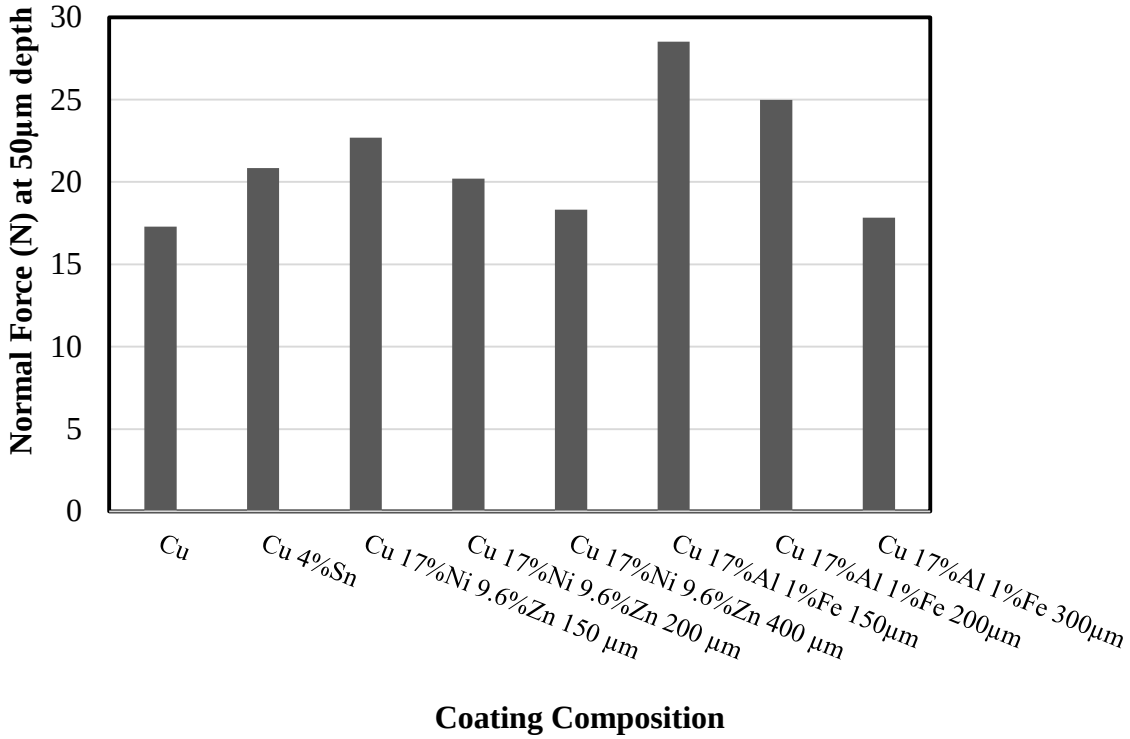

Figure 4-19 Critical loads required to penetrate the samples up to 50 µm.

4.6 Results of FE Modeling of Microindentation

As mentioned in section 3.5, 2-D axisymmetric model was utilized in the model. Figure 4-20 shows the stress around the indentation area for the four samples at the end of the simulated indentation process. It can be seen that the bottom surface of the coating material is not affected by the indentation process, which supports the assumption of excluding the substrate. It was observed from the model that plastic deformation takes place after the indenter comes in contact with the surface of the coating, evidenced by the fact that Von mises stress are higher than the yield strength of the materials. As the

indenter delves into the surface more and more, the zone of the plastic deformation expands vertically and horizontally until the indenter reaches the maximum depth, recording the maximum stresses and the widest plastic deformation zone. When the indenter starts to go back for the unloading step, elastic recovery takes place and the elastic stresses decrease to zero whereas the remaining permanent deformation makes the indent shape. Figure 4-20 shows that all coatings have the same deformation pattern and similar stress distribution, the only difference is the stress values.

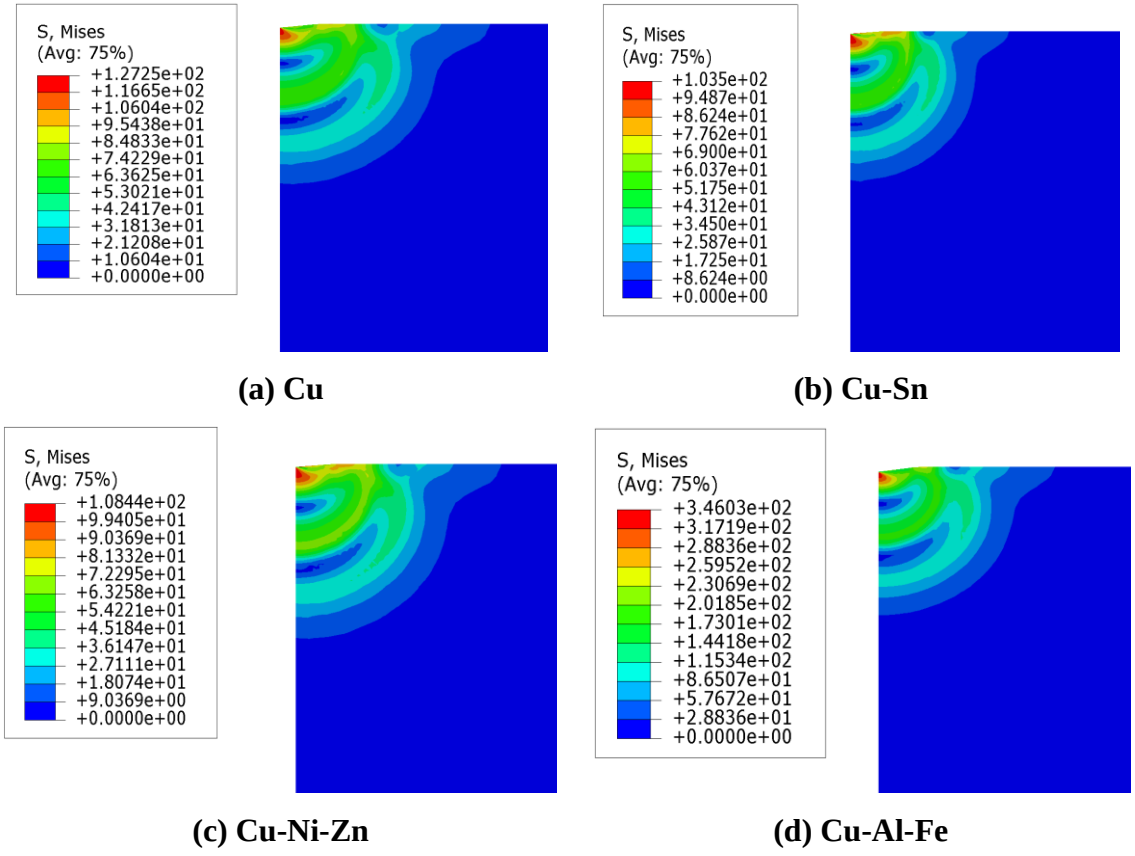

(a) Cu **(b) Cu-Sn**

(c) Cu-Ni-Zn **(d) Cu-Al-Fe**

Figure 4-20 Stresses around the indenter tip.

Figure 4-21 shows the force penetration curves from the experiments as well as from the model. It can be seen that close agreements between experiments and FE models have been achieved, especially in the first part of the unloading curve. This what was sought in

the first place, because Oliver & Pharr theory from which hardness and elastic-plastic properties are calculated as discussed in section 3.4.2 is based on the first part of the unloading curve in the force-penetration data. However, it has to be mentioned that significant elastic recovery was observed in the model compared to the experimental data. The tiny difference in the loading part of the force penetration curves can be ascribed to many factors including the experimental error and the fact that the experimental curves represent average values of many force penetration curves.

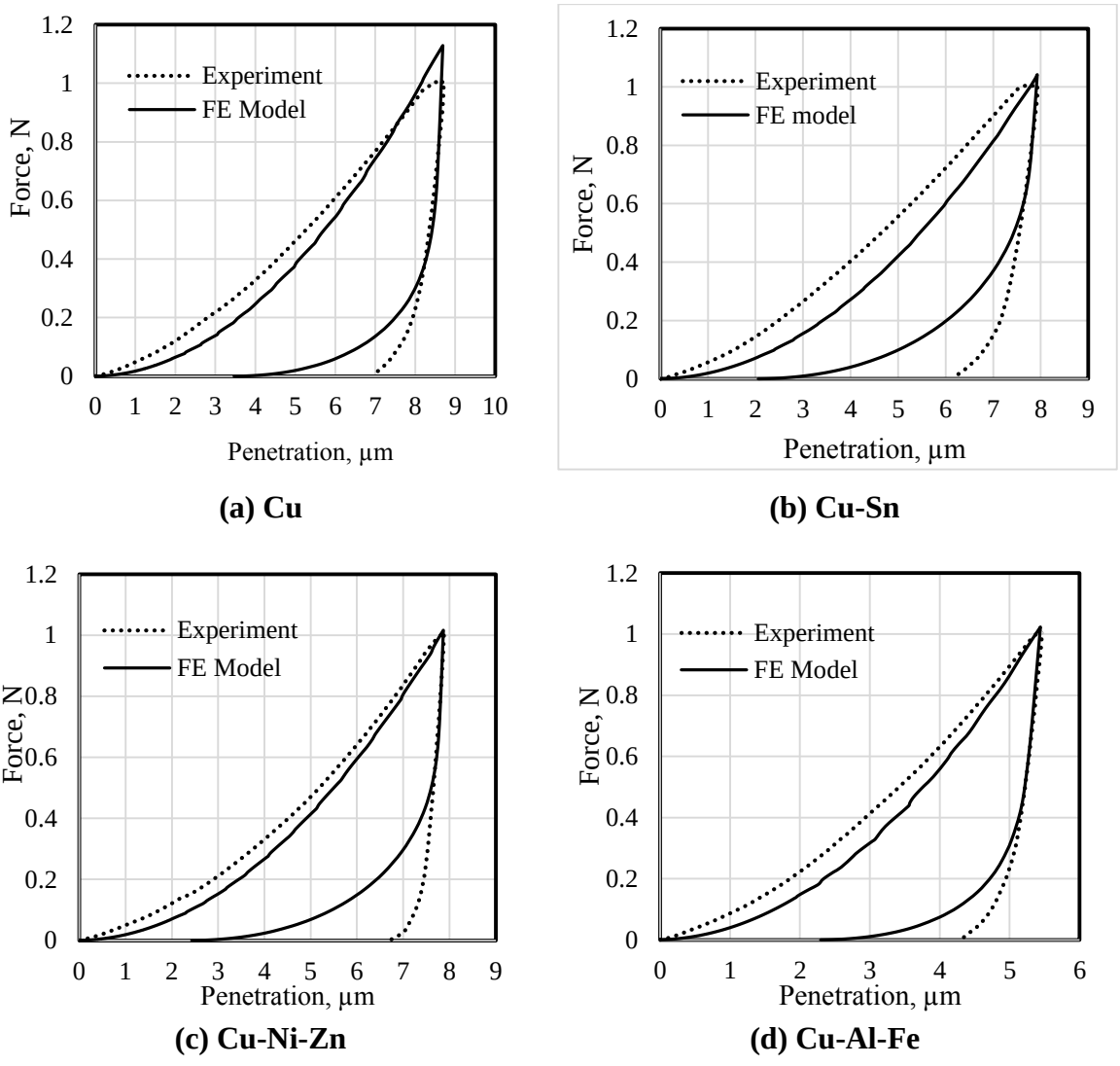

Figure 4-21 Matched Force-penetration curves.

Values of the Yield strength found from the model are listed in Table 4-4 along with the Young's modulus values. Values of Young's Modulus were extracted from the experiments as an average of many indentations using Oliver & Pharr theory as explained in section 3.4.2. Cu 17%Al 1%Fe samples have the highest Young's modulus whereas Cu 4%Sn have the lowest. It can be noticed that the values of Young's Modulus are lower than that of bulk materials (Young's Modulus of copper is 120 GPa). This can be ascribed to thermal spraying process, where these materials have undergone melting and solidification, which results in softening the materials and thereby reducing the Young's modulus.

Table 4-4 Yield Strength and Young's Modulus of the coating samples.

Coating composition	Young's Modulus (GPa)	Yield Strength (MPa)
Cu	60	94
Cu 4%Sn	49	75
Cu 17%Ni 10%Zn	57.5	86
Cu 17%Al 1%Fe	86.3	250

Now, since the elastic plastic responses of these materials are calibrated using the axisymmetric model of the indentation process, the stress-strain curve can be extracted from the calibrated material responses (Yield strength and the tangent modulus). The obtained stress-strain curves are shown in Figure 4-22.

It can be observed that Cu, Cu 4%Sn, and Cu 17%Ni 10Zn have close stress-strain curves indicating similar elastic-plastic responses. This can be evidenced by the values of yield

strength listed in Table 4-4. However, Cu 17%Al 1%Fe has a higher curve indicating high strength of the alloy. This confirms the results of the indentation and scratch tests where hardness and scratch resistance of this alloy was found to be high.

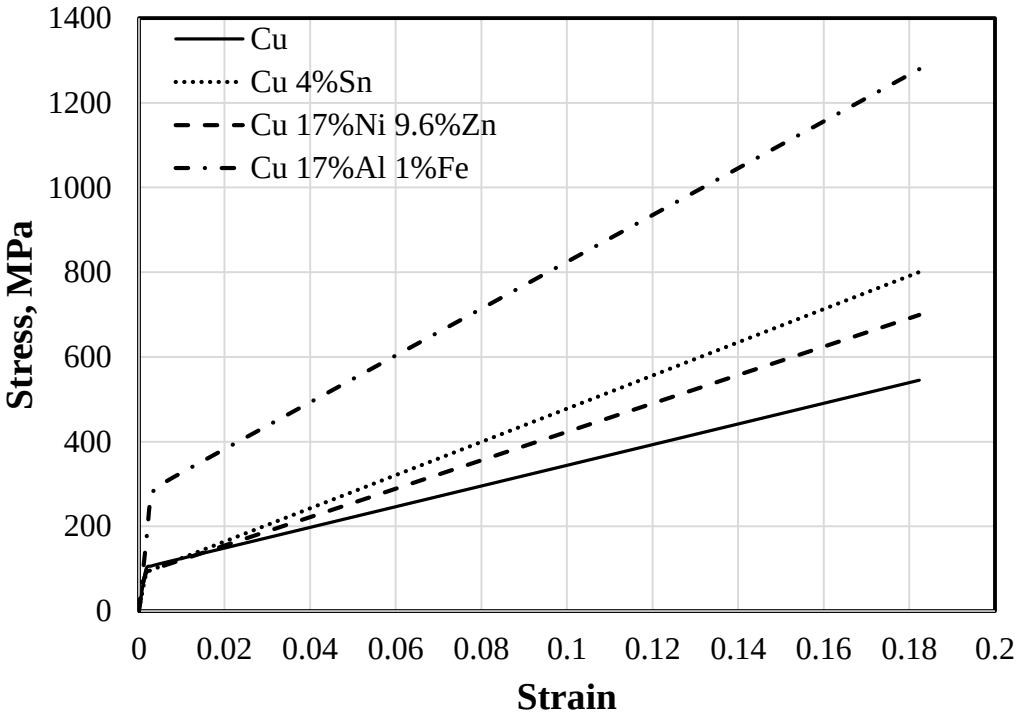

Figure 4-22 stress-strain curves from the FE modeling.

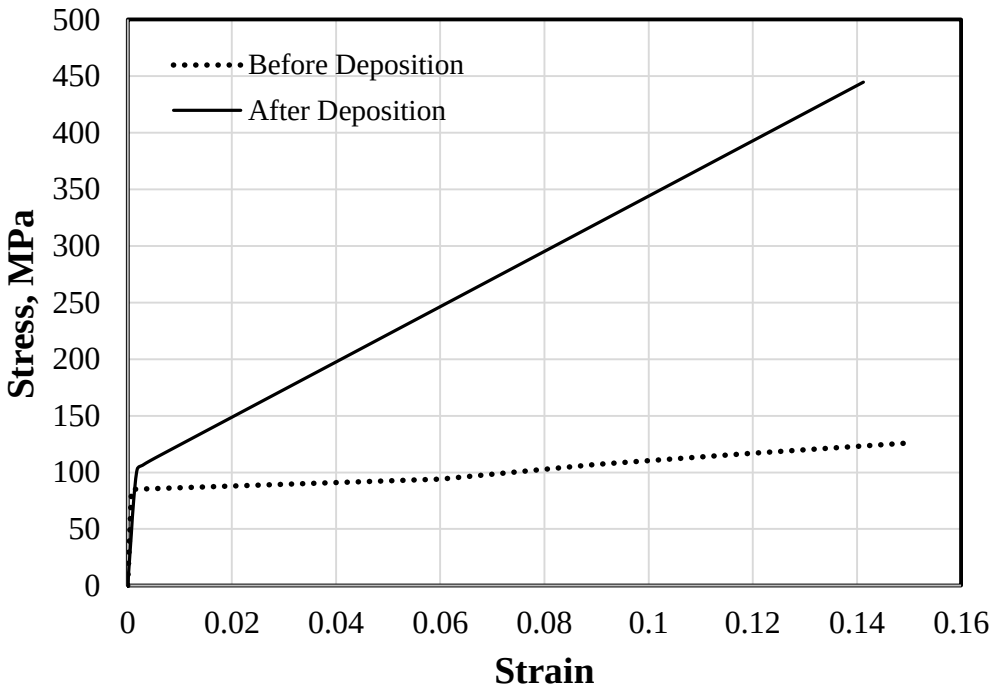

Figure 4-23 Comparison between bulk copper and thermal sprayed copper coating.

Figure 4-23 shows the engineering stress-strain curve of pure copper (99.99%) with pure copper coating after the deposition process. As anticipated, the thermal spraying process resulted in hardening copper, which is indicated by the high plastic response of the coating compared to the bulk material before deposition. It can also be observed that the Young's modulus of the coating has been reduced due to the deposition process.

The limitation of the model is that it neither considers the hardness trend of the cross section nor the effect of changing the thickness of the coating.

CHAPTER 5

CONCLUSIONS AND FUTURE WORK

In this chapter, the major findings of this study combined together are highlighted along with the recommendation of the study.

5.1 Effects of coating composition on the mechanical properties

As introduced before, mechanical properties (Adhesion strength, hardness, scratch resistance) of four different compositions (Cu, Cu 4%Sn, Cu 17%Ni 10%Zn, and Cu 17%Al 1%Fe) were studied.

As far as the coating composition is concerned, Cu 17%Al 1%Fe (Aluminum bronze) showed the highest interface adhesion strength compared to other composition. Part of the Aluminum bronze samples (those with lower thickness) had their adhesion strength that exceeded the strength of the epoxy glue. The strong bonding to the substrate surface of aluminum bronze coatings was anticipated by SEM micrographs of the interface before the adhesion test, where the SEM micrographs of the cross section showed that the aluminum bronze coatings are heavily deformed at the interface region in a manner that was not observed in other coating samples. Moreover, Cu 17%Al 1%Fe samples showed the highest hardness values measured by both, scratch and indentation. The mechanical superiority of the aluminum bronze coatings has been regarded to the components of the alloy, i.e. aluminum (Al) and iron (Fe), especially the high content of aluminum that could have only been achieved with thermal spraying.

For Cu 4%Sn coatings, relatively low adhesion strength values were found, and this was previously anticipated by the SEM cross-sectional micrographs, where clear cracks were seen at the interface, indicating poor adhesion of the coating to the surface of the substrate. Despite the fact that cracks were detected at the interface for tin bronze samples, the coating was found to be more integrate less porous, possibly because of the tin content in the alloy. This may be an indication to the fact that Cu 4%Sn samples, despite their low adhesion to the substrate, exhibit high cohesion strength between their splats. The integrity of the Cu 4%Sn samples led to their relatively high scratch and indentation hardness.

Cu 17%Ni 10%Zn samples showed moderate values of adhesion strength, indentation hardness, and scratch resistance compared to other coatings. For indentation hardness, some of Cu 17%Ni 10%Zn samples were found to have relatively hardness close to the interface region, a behavior that was not observed in other coatings. The instant drop in the interface hardness for this alloy was regarded to some of the cracks that were detected close to the interface, which may relieve the stresses that supposed to cause elevated hardness at the interface due to work hardening caused by intense plastic deformation.

5.2 Effects of coating thickness on the mechanical properties

Coating thickness was found to have great effects on the assessed mechanical properties. The role of the coating thickness can be understood by acknowledging the fact that changing the thickness of coating has substantial effects on the amount and distribution of residual stresses formed during the deposition process, which in turn, greatly influence the mechanical performance of the deposited coatings.

As the adhesion strength was assessed for different thickness for Cu 17%Ni 10%Zn and Cu 17%Al 1%Fe samples, it has been clearly demonstrated that the adhesion strength decreases with the coating thickness. This was regarded to the residual stress role in thicker coatings, for which, residual stresses act as driving force for the interface crack initiation and propagation. This was proven for Cu 17%Ni 10%Zn samples by SEM cross-sectional micrographs where the cracking intensity was found to increase with the coating thickness, and therefore, less bonding to the substrate surface is expected for higher thicknesses coatings. Thus, it can be postulated that thinner coatings are recommended for applications that require high interface adhesion.

On the other hand, coating hardness measured at cross section was found to increase with the coating thickness. The main reason for that, we argue, is the increase of residual stress level with the coating thickness, especially the component of residual stresses caused by thermal expansion mismatch between the coating and the substrate materials, as explained in section 4.4.3. Again, it has to be highlighted that the hardness is measured from the cross section of the sample, because if the hardness had to be checked at the top surface of the coatings, – which could not have been achieved because of the surface roughness – it would have been found to decrease with the coating thickness. This is because bulkier material complies easily to deformation.

Scratch hardness was found to increase with the coating thickness for Cu 17%Ni 10%Zn and Cu 17%Al 1%Fe samples possibly because of the residual stresses as indentation hardness. This is of practical importance since the thickness can be used as a criterion to increase the pencil (or scratch) hardness. However, surprisingly, the scratch resistance represented in terms of the force needed to penetrate the coating up to a certain depth was

found to decrease with the coating thickness, i.e. less force is required to penetrate a coating of a large thickness. This, although seems bizarre, can be related to the material compliance from the top surface for which, bulkier materials can easily be penetrated than thinner materials. One should carefully differentiate between resistance to scratch penetration and scratch hardness, as the latter is measured by considering the width produced by the indenter as it moves across the surface of the coating, and since the splats are by nature anisotropic, the force required to tear the coating would be different than that needed for penetration.

To conclude, for thermal spray metallic coating, high thickness is recommended for applications that require high scratch and indentation hardness, however, that will be associated with a degraded interface adhesion strength.

5.3 Future work

1. Residual stress measurements

   The mechanical properties of these alloys could be better understood if the residual stresses can be measured and the stress profile across the coating thickness can be defined. This can remarkably help in understanding the hardness profile, interface adhesion, and scratch resistance of the tested sample as well as understanding the role of the coating thickness in these properties. Therefore, measuring the residual stresses in these coating is advisable for further investigation.

2. Critical loads required to cause coating delamination

   As mentioned before, critical loads required to cause coating delamination have not been achieved due to force limitation of the scratch tester. Therefore, scratch tests

should be performed with larger forces to quantify the critical loads of delamination as well as to determine the scratch adhesion of these coatings.

3. Effect of coating composition

The effect of the coating composition on the mechanical properties can be further investigated for copper alloys (Bronzes) by examining different alloying percentages than the ones provided in this study.

4. Effect of the deposition process and deposition parameters

The effect of the deposition process and the deposition parameters on the quality of the coatings represented in good mechanical properties should be investigated in the future. This is motivated by the fact that deposition parameters have a great impact on the evolution of the coating microstructure as well as on residual stresses formed during the deposition process, both of which directly influence the mechanical properties of the coating.

References

[1] O. Sharifahmadian, H. R. Salimijazi, M. H. Fathi, J. Mostaghimi, and L. Pershin, "Relationship between surface properties and antibacterial behavior of wire arc spray copper coatings," *Surf. Coatings Technol.*, vol. 233, pp. 74–79, Oct. 2013.

[2] E. Zhang, F. Li, H. Wang, J. Liu, C. Wang, M. Li, and K. Yang, "A new antibacterial titanium-copper sintered alloy: preparation and antibacterial property.," *Mater. Sci. Eng. C. Mater. Biol. Appl.*, vol. 33, no. 7, pp. 4280–7, Oct. 2013.

[3] X. Jin, L. Gao, E. Liu, F. Yu, X. Shu, and H. Wang, "Microstructure, corrosion and tribological and antibacterial properties of Ti-Cu coated stainless steel.," *J. Mech. Behav. Biomed. Mater.*, vol. 50, pp. 23–32, Jun. 2015.

[4] H. Wu, X. Zhang, Z. Geng, Y. Yin, R. Hang, X. Huang, X. Yao, and B. Tang, "Preparation, antibacterial effects and corrosion resistant of porous Cu–TiO2 coatings," *Appl. Surf. Sci.*, vol. 308, pp. 43–49, Jul. 2014.

[5] S. Jaiswal, P. McHale, and B. Duffy, "Preparation and rapid analysis of antibacterial silver, copper and zinc doped sol-gel surfaces.," *Colloids Surf. B. Biointerfaces*, vol. 94, pp. 170–6, Jun. 2012.

[6] K.-D. Bouzakis, N. Michailidis, G. Skordaris, E. Bouzakis, D. Biermann, and R. M'Saoubi, "Cutting with coated tools: Coating technologies, characterization methods and performance optimization," *CIRP Ann. - Manuf. Technol.*, vol. 61, no. 2, pp. 703–723, Jan. 2012.

[7] M. R. Dorfman, *Handbook of Environmental Degradation of Materials*, Second Edi. Elsevier, 2012.

[8] L. Singh, V. Chawla, and J. S. Grewal, "A Review on Detonation Gun Sprayed Coatings," vol. 11, no. 3, pp. 243–265, 2012.

[9] C. M. Cotell, J. A. Sprague, F. A. Smidt, H. B. Sargent, O. H. Nestor, J. E. Pelton, and R. C. Eschenbach, "Thermal Spray Coatings," vol. 5, pp. 497–509, 2012.

[10] O. Sharifahmadian, H. R. Salimijazi, M. H. Fathi, J. Mostaghimi, and L. Pershin, "Relationship between surface properties and antibacterial behavior of wire arc spray copper coatings," *Surf. Coatings Technol.*, vol. 233, pp. 74–79, Oct. 2013.

[11] M. Miola, S. Perero, S. Ferraris, A. Battiato, C. Manfredotti, E. Vittone, D. Del Vento, S. Vada, G. Fucale, and M. Ferraris, "Silver nanocluster-silica composite antibacterial coatings for materials to be used in mobile telephones," *Appl. Surf. Sci.*, vol. 313, pp. 107–115, Sep. 2014.

[12] J. Li, B. Liu, H. Luo, Q. Fang, Y. Liu, and Y. Liu, "A molecular dynamics

investigation into plastic deformation mechanism of nanocrystalline copper for different nanoscratching rates," *Comput. Mater. Sci.*, vol. 118, pp. 66–76, 2016.

[13] D. V. Kudashov, R. Zauter, and H. R. Müller, "Spray-formed high-aluminium bronzes," *Mater. Sci. Eng. A*, vol. 477, no. 1–2, pp. 43–49, 2008.

[14] Z. Zhang, D. Li, and S. Wang, "High temperature performance of arc-sprayed aluminum bronze coatings for steel," *Trans. Nonferrous Met. Soc. China*, vol. 16, no. 4, pp. 868–872, Aug. 2006.

[15] H. Koivuluoto and P. Vuoristo, "Effect of Powder Type and Composition on Structure and Mechanical Properties of Cu + Al2O3 Coatings Prepared by using Low-Pressure Cold Spray Process," *J. Therm. Spray Technol.*, vol. 19, no. 5, pp. 1081–1092, Mar. 2010.

[16] K. I. Triantou, D. I. Pantelis, V. Guipont, and M. Jeandin, "Microstructure and tribological behavior of copper and composite copper+alumina cold sprayed coatings for various alumina contents," *Wear*, vol. 336–337, pp. 96–107, Aug. 2015.

[17] O. Culha, E. Celik, N. F. Ak Azem, I. Birlik, M. Toparli, and a. Turk, "Microstructural, thermal and mechanical properties of HVOF sprayed Ni–Al-based bond coatings on stainless steel substrate," *J. Mater. Process. Technol.*, vol. 204, no. 1–3, pp. 221–230, Aug. 2008.

[18] R. Guo, G. Yin, X. Sha, Q. Zhao, L. Wei, and H. Wang, "The significant adhesion enhancement of Ag–polytetrafluoroethylene antibacterial coatings by using of molecular bridge," *Appl. Surf. Sci.*, vol. 341, pp. 13–18, Jun. 2015.

[19] L. Jin, G. Liu, P. Li, H. Zhou, C. Wang, and G. Zhou, "Adhesion strength and thermal shock properties of nanostructured 5La3TiYSZ, 8LaYSZ and 8CeYSZ coatings prepared by atmospheric plasma spraying," *Ceram. Int.*, vol. 41, no. 9, pp. 12099–12106, Nov. 2015.

[20] W. Li, Y. Lu, K. Yuan, and C. Yuan, "Effects of cerium on microstructure and bonding strength of Cu-14Al-4.5Fe bronze plasma sprayed coating," *J. Rare Earths*, vol. 29, no. 4, pp. 363–369, Apr. 2011.

[21] H. Vakili, B. Ramezanzadeh, and R. Amini, "The corrosion performance and adhesion properties of the epoxy coating applied on the steel substrates treated by cerium-based conversion coatings," *Corros. Sci.*, vol. 94, pp. 466–475, May 2015.

[22] A. Vencl, S. Arostegui, G. Favaro, F. Zivic, M. Mrdak, S. Mitrović, and V. Popovic, "Evaluation of adhesion/cohesion bond strength of the thick plasma spray coatings by scratch testing on coatings cross-sections," *Tribol. Int.*, vol. 44, no. 11, pp. 1281–1288, Oct. 2011.

[23] M. J. Azizpour, H. Mohammadi, M. Jalali, and H. Fasihi, "Adhesion Strength Evaluation Methods in Thermally Sprayed Coatings," vol. 6, no. 1, pp. 1129–1131,

2012.

[24] J. M. Miguel, J. M. Guilemany, and S. Dosta, “Effect of the spraying process on the microstructure and tribological properties of bronze-alumina composite coatings,” *Surf. Coatings Technol.*, vol. 205, no. 7, pp. 2184–2190, 2010.

[25] P. D. Eason, J. a. Fewkes, S. C. Kennett, T. J. Eden, K. Tello, M. J. Kaufman, and M. Tiryakioğlu, “On the characterization of bulk copper produced by cold gas dynamic spray processing in as fabricated and annealed conditions,” *Mater. Sci. Eng. A*, vol. 528, no. 28, pp. 8174–8178, Oct. 2011.

[26] J. Qian, Y. Yin, T. Li, X. Hu, C. Wang, and S. Li, “Structure, micro-hardness and corrosion behaviour of the Al–Si/Al2O3 coatings prepared by laser plasma hybrid spraying on magnesium alloy,” *Vacuum*, vol. 117, pp. 55–59, 2015.

[27] S. Da Sun, D. Fabijanic, A. Ghaderi, M. Leary, J. Toton, S. Sun, M. Brandt, and M. Easton, “Microstructure and hardness characterisation of laser coatings produced with a mixture of AISI 420 stainless steel and Fe-C-Cr-Nb-B-Mo steel alloy powders,” *Surf. Coatings Technol.*, 2016.

[28] X. Guo, G. Zhang, W. Li, Y. Gao, H. Liao, and C. Coddet, “Investigation of the microstructure and tribological behavior of cold-sprayed tin-bronze-based composite coatings,” *Appl. Surf. Sci.*, vol. 255, no. 6, pp. 3822–3828, Jan. 2009.

[29] Y. Sun, T. Bell, and S. Zheng, “Finite element analysis of the critical ratio of coating thickness to indentation depth for coating property measurements by nanoindentation,” *Thin Solid Films*, vol. 258, no. 1–2, pp. 198–204, 1995.

[30] a. Bolshakov, W. C. Oliver, and G. M. Pharr, “Influences of stress on the measurement of mechanical properties using nanoindentation: Part II. Finite element simulations,” *J. Mater. Res.*, vol. 11, no. 03, pp. 760–768, 1996.

[31] C. K. S. Moy, M. Bocciarelli, S. P. Ringer, and G. Ranzi, “Indentation and imprint mapping for the identification of material properties in multi-layered systems,” *Comput. Mater. Sci.*, vol. 50, no. 5, pp. 1681–1691, 2011.

[32] Y. Xiao, W. Shi, and J. Luo, “Indentation for evaluating cracking and delamination of thin coatings using finite element analysis,” *Vacuum*, vol. 122, pp. 17–30, 2015.

[33] M. T. Tilbrook, D. J. Paton, Z. Xie, and M. Hoffman, “Microstructural effects on indentation failure mechanisms in TiN coatings: Finite element simulations,” *Acta Mater.*, vol. 55, no. 7, pp. 2489–2501, 2007.

[34] K. Holmberg, H. Ronkainen, A. Laukkanen, and K. Wallin, “Friction and wear of coated surfaces - scales, modelling and simulation of tribomechanisms,” *Surf. Coatings Technol.*, vol. 202, no. 4–7, pp. 1034–1049, 2007.

[35] K. Holmberg, A. Laukkanen, H. Ronkainen, K. Wallin, and S. Varjus, “A model for stresses, crack generation and fracture toughness calculation in scratched TiN-coated steel surfaces,” *Wear*, vol. 254, no. 3–4, pp. 278–291, 2003.

[36] Y. Sun, A. Bloyce, and T. Bell, “Finite element analysis of plastic deformation of various TiN coating/ substrate systems under normal contact with a rigid sphere,” *Thin Solid Films*, vol. 271, no. 1–2, pp. 122–131, 1995.

[37] J. Michler and E. Blank, “Analysis of coating fracture and substrate plasticity induced by spherical indentors: Diamond and diamond-like carbon layers on steel substrates,” *Thin Solid Films*, vol. 381, no. 1, pp. 119–134, 2001.

[38] X. Zhao, Z. Xie, and P. Munroe, “Nanoindentation of hard multilayer coatings: Finite element modelling,” *Mater. Sci. Eng. A*, vol. 528, no. 3, pp. 1111–1116, 2011.

[39] P. S. Pandure, V. S. Jatti, and T. P. Singh, “Finite element simulation of nano-indentation of DLC coated HSS substrate,” *Procedia Mater. Sci.*, vol. 6, no. Icmpc, pp. 1619–1624, 2014.

[40] P. P. Liu, F. R. Wan, and Q. Zhan, “A model to evaluate the nano-indentation hardness of ion-irradiated materials,” *Nucl. Instruments Methods Phys. Res. Sect. B Beam Interact. with Mater. Atoms*, vol. 342, pp. 13–18, 2015.

[41] M. Lichinchi, C. Lenardi, J. Haupt, and R. Vitali, “Simulation of Berkovich nanoindentation experiments on thin films using finite element method,” *Thin Solid Films*, vol. 333, no. 1–2, pp. 278–286, 1998.

[42] A. A. Pelegri and X. Huang, “Nanoindentation on soft film/hard substrate and hard film/soft substrate material systems with finite element analysis,” *Compos. Sci. Technol.*, vol. 68, no. 1, pp. 147–155, 2008.

[43] J. D. Bressan, A. Tramontin, and C. Rosa, “Modeling of nanoindentation of bulk and thin film by finite element method,” *Wear*, vol. 258, no. 1–4 SPEC. ISS., pp. 115–122, 2005.

[44] R. D. Jamison and Y.-L. Shen, “Delamination analysis of metal–ceramic multilayer coatings subject to nanoindentation,” *Surf. Coatings Technol.*, 2016.

[45] D. E. Vlachos, Y. P. Markopoulos, and V. Kostopoulos, “3-D modeling of nanoindentation experiment on a coating-substrate system,” *Comput. Mech.*, vol. 27, no. 2, pp. 138–144, 2001.

[46] L. Bartolomé, E. Oblak, and M. Kalin, “Mechanical behaviour and constitutive models of ZDDP tribofilms on DLC coatings using nano-indentation data and finite element modelling,” *Tribol. Int.*, vol. 95, pp. 19–26, 2016.

[47] A. Karimzadeh, M. R. Ayatollahi, and M. Alizadeh, “Finite element simulation of nano-indentation experiment on aluminum 1100,” *Comput. Mater. Sci.*, vol. 81, pp. 595–600, 2014.

[48] A. Wagih and A. Fathy, “Experimental investigation and FE simulation of nano-indentation on Al–Al2O3 nanocomposites,” *Adv. Powder Technol.*, 2016.

[49] Y. Fizi, Y. Mebdoua, H. Lahmar, S. Djeraf, and S. Benbahouche, “Adhesion of FeCrNiBSi-(W-Ti)C wire-arc deposited coatings onto carbon steel substrates determined by indentation measurements and modeling,” *Surf. Coatings Technol.*, vol. 268, pp. 310–316, 2015.

[50] M. Kot, W. Rakowski, J. M. Lackner, and Ł. Major, “Analysis of spherical indentations of coating-substrate systems: Experiments and finite element modeling,” *Mater. Des.*, vol. 43, pp. 99–111, 2013.

[51] M.-J. Pac, S. Giljean, C. Rousselot, F. Richard, and P. Delobelle, “Microstructural and elasto-plastic material parameters identification by inverse finite elements method of Ti(1−x)AlxN (0<x<1) sputtered thin films from Berkovich nano-indentation experiments,” *Thin Solid Films*, vol. 569, pp. 81–92, 2014.

[52] S. J. Bull and E. G.-Berasetegui E., *Chapter 7 An overview of the potential of quantitative coating adhesion measurement by scratch testing*, vol. 51, no. February. Elsevier Masson SAS, 2006.

[53] D. Beegan, S. Chowdhury, and M. T. Laugier, “Comparison between nanoindentation and scratch test hardness (scratch hardness) values of copper thin films on oxidised silicon substrates,” *Surf. Coatings Technol.*, vol. 201, no. 12, pp. 5804–5808, 2007.

[54] M. Barletta, V. Tagliaferri, A. Gisario, and S. Venettacci, “Progressive and constant load scratch testing of single- and multi-layered composite coatings,” *Tribol. Int.*, vol. 64, pp. 39–52, 2013.

[55] T. Futami, M. Ohira, H. Muto, and M. Sakai, “Contact/scratch-induced surface deformation and damage of copper-graphite particulate composites,” *Carbon N. Y.*, vol. 47, no. 11, pp. 2742–2751, 2009.

[56] S. Roy, E. Darque-Ceretti, E. Felder, F. Raynal, and I. Bispo, “Experimental analysis and finite element modelling of nano-scratch test applied on 40-120 nm SiCN thin films deposited on Cu/Si substrate,” *Thin Solid Films*, vol. 518, no. 14, pp. 3859–3865, 2010.

[57] N. X. Randall, G. Favaro, and C. H. Frankel, “The effect of intrinsic parameters on the critical load as measured with the scratch test method,” *Surf. Coatings Technol.*, vol. 137, no. 2–3, pp. 146–151, 2001.

[58] A. Ghabchi, S. Sampath, K. Holmberg, and T. Varis, “Damage mechanisms and cracking behavior of thermal sprayed WC-CoCr coating under scratch testing,” *Wear*, vol. 313, no. 1–2, pp. 97–105, 2014.

[59] N. I. Tymiak, D. E. Kramer, D. F. Bahr, T. J. Wyrobek, and W. W. Gerberich, “Plastic strain and strain gradients at very small indentation depths,” *Acta Mater.*, vol. 49, no. 6, pp. 1021–1034, 2001.

[60] T. Chudoba and F. Richter, “Investigation of creep behaviour under load during

indentation experiments and its influence on hardness and modulus results," *Surf. Coatings Technol.*, vol. 148, no. 2–3, pp. 191–192, 2001.

[61] D. A. Lucca, K. Herrmann, and M. J. Klopfstein, "Nanoindentation: Measuring methods and applications," *CIRP Ann. - Manuf. Technol.*, vol. 59, no. 2, pp. 803–819, 2010.

[62] W. C. Oliver and G. M. Pharr, "Measurement of hardness and elastic modulus by instrumented indentation: Advances in understanding and refinements to methodology," *J. Mater. Res.*, vol. 19, no. 01, pp. 3–20, 2004.

[63] a O. Sergici and X. N. Randall, "Scratch Testing of Coatings.(TECH SPOTLIGHT)," *Adv. Mater. Process.*, no. April, pp. 41–43, 2006.

[64] S. Deshpande, S. Sampath, and H. Zhang, "Mechanisms of oxidation and its role in microstructural evolution of metallic thermal spray coatings—Case study for Ni–Al," *Surf. Coatings Technol.*, vol. 200, no. 18–19, pp. 5395–5406, May 2006.

[65] J. Alcala, "Instrumented spherical micro-indentation of plasma-sprayed coatings," vol. 316, pp. 1–10, 2001.

[66] R. a. Neiser, M. F. Smith, and R. C. Dykhuizen, "Oxidation in Wire HVOF-Sprayed Steel," *J. Therm. Spray Technol.*, vol. 7, no. 4, pp. 537–545, Dec. 1998.

[67] P. M.P., H. Liao, and C. Coddet, "Relationships between in-flight particle characteristics and coating microstructure with a twin wire arc spray process and different working conditions," *Surf. Coatings Technol.*, vol. 182, no. 2–3, pp. 215–226, Apr. 2004.

[68] N. Pistofidis, G. Vourlias, E. Pavlidou, P. Patsalas, G. Stergioudis, and E. K. Polychroniadis, "Study of the structure and morphology of plasma-sprayed tin coating.pdf," vol. 200, pp. 6245–6250, 2006.

[69] M. Hadad, G. Marot, P. Démarécaux, J. Lesage, J. Michler, and S. Siegmann, "Adhesion tests for thermal spray coatings : Application range of tensile , shear and interfacial indentation methods G residual =," pp. 759–764, 2005.

[70] D. J. Greving, J. R. Shadley, and E. F. Rybicki, "C633-79 Thermal Spray Coating Test Specimens," vol. 3, no. December, pp. 371–378, 1994.

[71] D. Chicot, H. Ageorges, M. Voda, G. Louis, M. A. Ben Dhia, C. C. Palacio, and S. Kossman, "Hardness of thermal sprayed coatings: Relevance of the scale of measurement," *Surf. Coatings Technol.*, vol. 268, pp. 173–179, 2015.

[72] Z. Chen and L. Y. L. Wu, *Scratch damage resistance of silica-based sol-gel coatings on polymeric substrates*, Second Edi. Elsevier, 2013.

Vitae

Name :MOHAMED ELHADI MOHAMED IBRAHIM

Nationality :SUDANESE

Date of Birth :8/10/1991

Email : mho.elhadi8@gmail.com

Address : 29st, Al-Doha, Omdurman, Khartoum, Sudan.

Academic Background :

M.Sc. Mechanical Engineering, King Fahd University of Petroleum and Minerals, Saudi Arabia (2016)

B.Sc. Mechanical Engineering, University of Khartoum, Sudan (2012)

Work Experience **:**

Teaching Assistant (2012 – 2014), University of Khartoum, Sudan.